Weierstraß-Institut

für Angewandte Analysis und Stochastik

Leibniz-Institut im Forschungsverbund Berlin e. V.

Preprint ISSN 0946 – 8633

Coherence-incoherence patterns in a ring of non-locally coupled phase oscillators

Oleh Omel'chenko

submitted: April 15, 2013

Weierstrass Institute
Mohrenstr. 39
10117 Berlin
Germany
E-Mail: Oleh.Omelchenko@wias-berlin.de

No. 1777

Berlin 2013

2010 *Mathematics Subject Classification.* 34C15, 35B36, 35B32, 35B42, 35Q83.

2008 *Physics and Astronomy Classification Scheme.* 05.45.Xt, 89.75.Kd.

Key words and phrases. Coupled phase oscillators, non-local coupling, coherence-incoherence patterns, chimera states, bifurcation analysis, pattern formation.

Edited by
Weierstraß-Institut für Angewandte Analysis und Stochastik (WIAS)
Leibniz-Institut im Forschungsverbund Berlin e. V.
Mohrenstraße 39
10117 Berlin
Germany

Fax: +49 30 20372-303
E-Mail: preprint@wias-berlin.de
World Wide Web: http://www.wias-berlin.de/

Abstract

We consider a paradigmatic spatially extended model of non-locally coupled phase oscillators which are uniformly distributed within a one-dimensional interval and interact depending on the distance between their sites modulo periodic boundary conditions. This model can display peculiar spatio-temporal patterns consisting of alternating patches with synchronized (coherent) or irregular (incoherent) oscillator dynamics, hence the name coherence-incoherence pattern, or chimera state. For such patterns we formulate a general bifurcation analysis scheme based on a hierarchy of continuum limit equations. This gives us possibility to classify known coherence-incoherence patterns and to suggest directions for searching new ones.

1 Introduction

Emergence of collective behavior (synchrony) in large groups of oscillators plays an important role in a wide variety of significant applications. Examples are synchronization of neuronal oscillations in brain [1, 2, 3], entrainment in coupled Belousov-Zhabotinsky chemically reacting cells [4, 5], Josephson junction circuits [6] and mode-locked lasers [7], other references also can be found in [8]. It is well-known that in the context of N weakly coupled oscillators [9, 10], main features of synchronization phenomenon can be adequately reproduced by a corresponding phase reduced model

$$\frac{d\theta_k}{dt} = \omega_k - \frac{1}{N}\sum_{j=1}^{N} G_{kj} F(\theta_k(t) - \theta_j(t)), \qquad k = 1, \ldots, N, \tag{1}$$

where the state of the k-th oscillator is represented solely by its scalar phase $\theta_k \in \mathbb{R}$. Further, natural frequencies $\omega_k \in \mathbb{R}$ reflect the individual differences between oscillators, and a coupling matrix $G_{kj} \in \mathbb{R}^{N\times N}$ together with a 2π-periodic function $F : \mathbb{R} \to \mathbb{R}$ determine the details of interaction between oscillators. To get a qualitative insight into model (1) it is often enough to replace a particular function F with its leading Fourier harmonics of the form $\sin(\theta + \alpha)$ where $\alpha \in \mathbb{R}$ is referred to as *phase lag* parameter. In the case of *global* coupling (when all G_{kj} are equal) and natural frequencies ω_k drawn from a certain probability distribution, this simplification gives a paradigmatic Kuramoto-Sakaguchi model [11] that describes synchronization transition in a homogeneous bulk. However, bulk approximation is not always suitable. For many spatially extended systems, it appears more natural to assume that coupling coefficients G_{kj} vary depending on real physical distance between oscillators. To mimic this feature Kuramoto and Battogtokh suggested in [12] another kind of model (1) that reads

$$\frac{d\theta_k}{dt} = \omega - \frac{2\pi}{N}\sum_{j=1}^{N} G_{kj} \sin(\theta_k(t) - \theta_j(t) + \alpha), \qquad k = 1, \ldots, N. \tag{2}$$

Here all oscillators have the same natural frequency $\omega \in \mathbb{R}$ and are equipped with additional spatial labels x_k denoting their positions within the one-dimensional reference interval $[-\pi, \pi]$, hence the normalization prefactor 2π at the sum. Assuming that x_k are uniformly distributed over $[-\pi, \pi]$ (typical choice is $x_k = -\pi + 2\pi k/N$), one defines

$$G_{kj} = G(x_k - x_j), \tag{3}$$

where $G : \mathbb{R} \to \mathbb{R}$ is a continuous even and 2π-periodic *coupling function* introducing a symmetric ring coupling topology between oscillators. If G is constant and non-zero then Eq. (3) determines global coupling. On the other hand, any non-constant function G produces a qualitatively different coupling topology which according to established tradition is called *non-local* coupling. The non-local coupling is defined on a macroscopic level, hence using a particular function G one obtains a sequence of systems (2)–(3) with different sizes N. Nevertheless for sufficiently large N all these systems demonstrate macroscopically similar long-term dynamics. In particular, starting from randomly chosen initial conditions and simulating system (2)–(3) one typically obtains either a completely synchronized solution, Fig. 1 (a), or a twisted phase-locked solution, Fig. 1 (b). However, it was an exciting discovery that in spite of apparent structural symmetry, for some parameter values system (2)–(3) can also support unexpected spatio-temporal patterns shown in Fig. 1 (c) where synchronized (*coherent*) and irregular (*incoherent*) oscillator dynamics is observed simultaneously but at different sites x_k. Such *coherence-incoherence patterns* attracted great interest and have been the subject of numerous studies in last decade [12, 13, 14, 15, 16, 17, 18, 19, 20, 21, 22, 23, 24, 25, 26, 27, 28, 29, 30]. In most of above publications they are referred to as *chimera states*. This name sounds attractive but is very loosely defined. For example, it was used to denote asymmetric partially synchronized states in two or three interacting groups of globally coupled oscillators [31, 32], or to denote non-trivial fixed points in networks of non-locally coupled maps [33, 34]. Therefore, in order to identify more precisely the main object of our study we intentionally use the name coherence-incoherence pattern instead of chimera state.

To the best of our knowledge, all previous studies of coherence-incoherence patterns were concerned with a particular choice of coupling function G. Kuramoto and Battogtokh considered an exponential coupling [12] of the form

$$G(x) \sim e^{-\kappa|x|} \quad \text{with} \quad \kappa > 0$$

motivated by adiabatic elimination of fast diffusive variable in a multi-component oscillatory chemical system. A few years later, the cosine coupling

$$G(x) = \frac{1}{2\pi}(1 + A\cos x) \quad \text{with} \quad A \in (0, 1) \tag{4}$$

was suggested [14, 15] in order to simplify the mathematical complexity of the problem. Finally, the piecewise-constant coupling with a radius $r \in (0, 1)$

$$G(x) = \begin{cases} (2\pi r)^{-1} & \text{for} \quad |x| \le \pi r, \\ 0 & \text{for} \quad |x| > \pi r \end{cases} \tag{5}$$

was used in [23, 25, 26] to study the dynamical nature of coherence-incoherence patterns in the context of finite size systems.

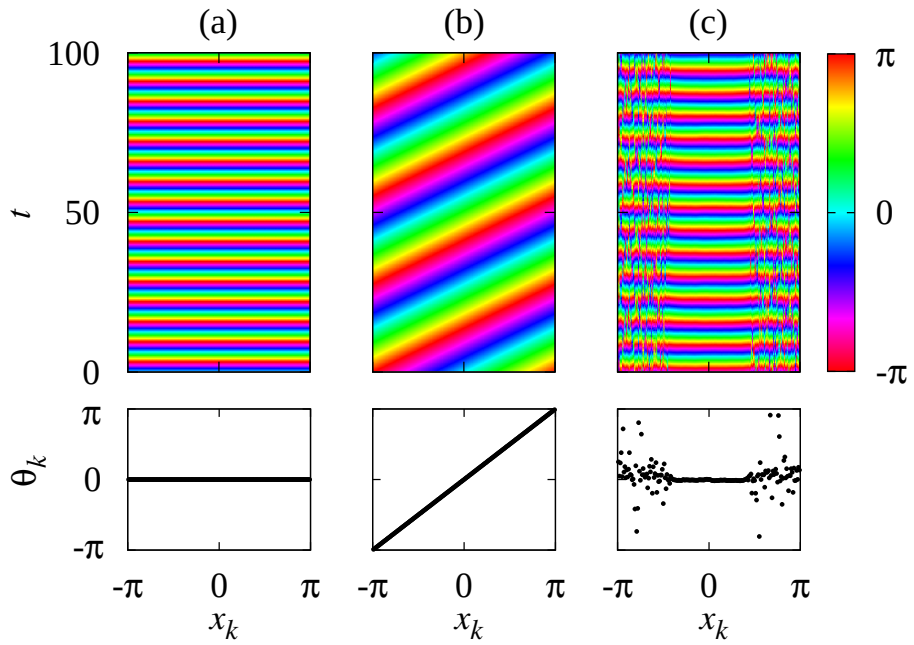

Figure 1: Solutions observed in numerical simulations of Eqs. (2)–(3): (a) completely synchronized state, (b) twisted state, and (c) coherence-incoherence pattern. Top and bottom panels display time dynamics of oscillators and corresponding instantaneous snapshots, respectively. Translational symmetry of Eqs. (2)–(3) was used to center the resulting plots. Parameters: $N = 200, \omega = 0, \alpha = \pi/2 - 0.1$, and piecewise-constant coupling (5) with $r = 0.8$. Each solution can be approached with a nonvanishing probability starting from randomly chosen initial data.

In contrast, this work focuses on the systematic description of coherence-incoherence patterns and other dynamical regimes observed in system (2)–(3) after an initial transient for arbitrary choice of coupling function G. For this we employ the large N limit formalism explained in Section 2. There, applying the ideas of the Ott-Antonsen invariant manifold theory we show that on a macroscopic level the effective dynamics of system (2)–(3) can be described in terms of a complex-valued function — local order parameter, that evolves according to some explicitly known equation in Banach space of continuous functions. It turns out that coherence-incoherence patterns as well as completely synchronized and twisted solutions can be represented as standing wave solutions of the latter equation. Moreover, spatially dependent amplitudes of these waves and their rotational frequencies satisfy a nonlinear integral equation with $O(2) \times S^1$-symmetry, which has a form of the infinite-dimensional nonlinear eigenvalue problem (NEVP). In Section 3 we perform a detailed analysis of the solution set to this NEVP. In particular, we show that every non-zero harmonics in the Fourier series of coupling function G gives rise to several solution curves (modulo the symmetry group action) organized as primary an secondary branches bifurcating from the trivial solution. All the branches can be interpreted either as coherence-incoherence patterns or as phase-locked solutions of system (2)–(3). Remarkably, only a few of them are stable and can be observed in numerical simulations. The underlying stability analysis with respect to the evolution equation for local order parameter is addressed in Section 4. Discussion and concluding remarks are presented in Section 5.

Notations. Throughout this paper we assume the following notations. For any integer $k \geq 0$, by $C^k_{\rm per}([-\pi,\pi];\mathbb{R})$ and $C^k_{\rm per}([-\pi,\pi];\mathbb{C})$ we denote the Banach spaces of 2π-periodic, real- and complex-valued functions, respectively, which are continuous together with their derivatives up to the k-th order. These spaces are equipped with their usual supremum norms

$$\|u\|_k := \|u\|_{C^k_{\rm per}([-\pi,\pi];\mathbb{R})} = \|u\|_{C^k_{\rm per}([-\pi,\pi];\mathbb{C})} = \max_{x\in[-\pi,\pi]} \sum_{j=0}^{k} |u^{(j)}(x)|.$$

Instead of $C^0_{\rm per}([-\pi,\pi];\mathbb{R})$ and $C^0_{\rm per}([-\pi,\pi];\mathbb{C})$ we use notations $C_{\rm per}([-\pi,\pi];\mathbb{R})$ and $C_{\rm per}([-\pi,\pi];\mathbb{C})$, respectively.

In some cases we identify function $u \in C^k_{\rm per}([-\pi,\pi];\mathbb{C})$ with a vector-function of its real and imaginary parts

$$(\operatorname{Re} u, \operatorname{Im} u)^{\rm T} \in C^k_{\rm per}([-\pi,\pi];\mathbb{R}^2)$$

that simultaneously provides a natural definition of the latter Banach space. Then for a mapping

$$\mathcal{F} : \mathbb{R}^2 \ni (u_1,u_2)^{\rm T} \mapsto (f_1(u_1,u_2), f_2(u_1,u_2))^{\rm T} \in \mathbb{R}^2$$

where f_1 and f_2 are given smooth functions, we use an equivalent complex notation

$$u = u_1 + iu_2 \mapsto f(u) = f_1(u_1,u_2) + if_2(u_1,u_2) \quad \text{with} \quad f : \mathbb{C} \to \mathbb{C}.$$

This notation implies a simple formula for derivative of $\mathcal{F}$ (in the $\mathbb{R}^2$-topology) that reads

$$\mathcal{F}'(u)v = \frac{d}{dt} f(u+tv)\bigg|_{t=0}. \tag{6}$$

Finally, for any $u, v \in C_{\rm per}([-\pi,\pi];\mathbb{C})$ we define the inner product

$$\langle u, v\rangle := \int_{-\pi}^{\pi} \overline{u}(x)v(x)dx, \tag{7}$$

where $\overline{u}$ denotes the complex conjugate of u.

2 Continuum limit approach

Completely synchronized and twisted solutions of Eqs. (2)–(3) are known explicitly, therefore their dynamical properties can be analyzed in the framework of this finite-dimensional system [35, 36]. In contrary, numerical simulations demonstrate [26] that coherence-incoherence patterns are hyper-chaotic trajectories with the number of positive Lyapunov exponents being proportional to the system size N. For increasing N such patterns seem to become tremendously complicated objects. However, this is not the case. In fact their macroscopic dynamics for $N \to \infty$ turns out to be in a certain sense equivalent to the dynamics of a periodic orbit of some deterministic infinite-dimensional evolution equation.

2.1 Continuum limit equation

If $N \to \infty$ then instead of looking for individual phases $\theta_k(t)$ we may look for their probability distribution $f(\theta, x, t)$, which for fixed time t gives a relative number of oscillators with $\theta_k(t) \approx \theta$ and $x_k \approx x$. Evolution equation for distribution f can be derived phenomenologically as we explain below. Its rigorous justification is more involved and can be found somewhere else, see for example recent work of Luçon and Stannat [37].

First, we rewrite Eq. (2) in a local form

$$\frac{d\theta_k}{dt} = \omega + \operatorname{Im}\left(Z_k(t)e^{-i(\theta_k(t)+\alpha)}\right), \quad k = 1, \dots, N, \tag{8}$$

where each phase θ_k is coupled solely with the averaged driving force

$$Z_k(t) = \frac{2\pi}{N}\sum_{j=1}^{N} G_{kj}e^{i\theta_j(t)}.$$

For $N \to \infty$, the latter sum can be formally replaced with a value of integral

$$Z(x,t) = \int_{-\pi}^{\pi} G(x-y)\int_0^{2\pi} f(\theta, y, t)e^{i\theta}\, d\theta\, dy \tag{9}$$

evaluated at the position of the k-th oscillator $x = x_k$. Suppose for a moment that all $Z_k(t) = Z(x_k, t)$ are known, then dynamics of f corresponding to Eq. (8) has to obey a continuity equation

$$\frac{\partial f}{\partial t} + \frac{\partial}{\partial \theta}(fJ) = 0, \tag{10}$$

where

$$J(\theta, x, t) = \omega + \operatorname{Im}\left(Z(x,t)e^{-i(\theta+\alpha)}\right) \tag{11}$$

is the right-hand side of Eq. (8). However in our case $Z(x,t)$ is not given rather depends on f, see (9). Hence self-consistent dynamics of probability distribution f is governed by the nonlinear integro-differential equation (10)–(11) where $Z(x,t)$ is expressed by formula (9). Note the integral term of Eq. (10) is hidden in formula (9) whereas quadratic nonlinearity appears from the product fJ. Following established tradition we call Eqs. (10)–(11) the *continuum limit equation*.

2.2 Ott-Antonsen invariant manifold and local order parameter

Direct study of continuum limit equation is quite a difficult task, in particular because its solutions typically are generalized functions, or measures. Already in the case of bulk synchronization, bifurcation analysis of continuum limit equation is so complicated [38, 39] that most of interesting facts about the qualitative behaviour of its solutions turn out to be hidden behind mathematical details. Fortunately, the fact that phase interaction in Eq. (2) is given by a pure sinusoidal term allows us to simplify the analysis of Eqs. (10)–(11) significantly. To this end, we use the Ott-Antonsen method suggested in [40, 41]. Roughly speaking it says that Eqs. (10)–(11) have an explicitly known attracting invariant manifold that contains all relevant dynamics of Eqs. (2)–(3) for large N. Exact form of this manifold is described in the following lemma.

Lemma 1 *Suppose that:*

(i) $z(x,\cdot) \,:\, [0,\infty) \to C_{\rm per}([-\pi,\pi];\mathbb{C})$ *satisfies the inequality* $|z(x,t)|<1$*,*

(ii) $z(x,t)$ *is a solution of the equation*

$$\frac{dz}{dt} = i\omega z(x,t) + \frac{1}{2}e^{-i\alpha}\mathcal{G}z - \frac{1}{2}e^{i\alpha}z^2(x,t)\mathcal{G}\overline{z}, \tag{12}$$

where $\mathcal{G} \,:\, C_{\rm per}([-\pi,\pi];\mathbb{C}) \to C_{\rm per}([-\pi,\pi];\mathbb{C})$ *is an integral convolution operator defined by*

$$(\mathcal{G}\varphi)(x) := \int_{-\pi}^{\pi} G(x-y)\varphi(y)dy. \tag{13}$$

Then, probability distribution f *given by*

$$f(\theta,x,t) = \frac{1}{2\pi}\left(1 + \sum_{n=1}^{\infty}\left[\overline{z}^n(x,t)e^{in\theta} + z^n(x,t)e^{-in\theta}\right]\right), \tag{14}$$

is a solution of the continuum limit equation (10)–(11).

Proof: For $|z|<1$ the series in the right-hand side of (14) converges absolutely. Substituting this into Eqs. (10)–(11) and reordering terms appropriately we obtain

$$\begin{aligned}\frac{\partial f}{\partial t} + \frac{\partial}{\partial\theta}(fJ) &= \frac{1}{2\pi}\left(\frac{dz}{dt} - i\omega z - \frac{1}{2}e^{-i\alpha}\mathcal{G}z + \frac{1}{2}e^{i\alpha}z^2\mathcal{G}\overline{z}\right)\sum_{n=1}^{\infty} nz^{n-1}e^{-in\theta} \\ &+ \frac{1}{2\pi}\left(\frac{d\overline{z}}{dt} + i\omega\overline{z} - \frac{1}{2}e^{i\alpha}\mathcal{G}\overline{z} + \frac{1}{2}e^{-i\alpha}\overline{z}^2\mathcal{G}z\right)\sum_{n=1}^{\infty} n\overline{z}^{n-1}e^{in\theta}.\end{aligned}$$

Clearly, if z satisfies Eq. (12) then each expression in parenthesis vanishes and hence Eq. (10) is fulfilled. •

Remark 1 *Eq. (12) was first obtained by Laing in [20]. Later on, we pointed out [26] an alternative way to derive it using the Watanabe-Strogatz ansatz in the context of hierarchical populations of coupled oscillators, see [42, 43] for detail.*

Distribution f defined by formula (14) has a clear interpretation with respect to the complex-valued function z. Indeed for any $|z(x,t)|<1$, summation in (14) yields

$$P_z(\theta) = \frac{1}{2\pi}\frac{1-|z|^2}{1-2|z|\cos(\theta-\arg z)+|z|^2}$$

that is a Poissonian distribution in the phase θ (see Fig. 2). In particular, $\arg z$ indicates the location of its center, whereas $|z|$ characterizes the degree of non-uniformity of this distribution. For $|z|=1$, distribution (14) degenerates into a delta function

$$P_z(\theta) = \delta(\theta - \arg z),$$

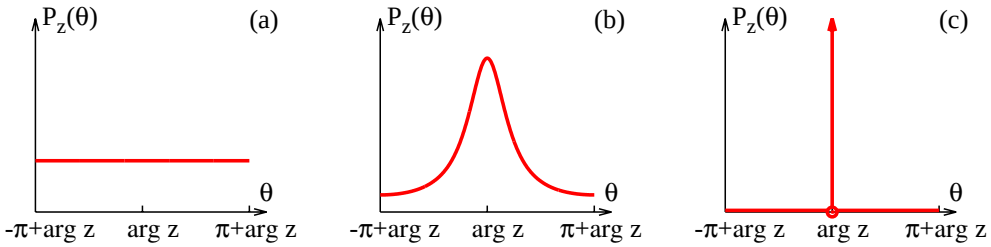

Figure 2: Poissonian distributions $P_z(\theta)$ for (a): $|z| = 0$, (b): $0 < |z| < 1$, and (c): $|z| = 1$.

therefore we call oscillators with sites $x_k \approx x$ *coherent*. In contrary, oscillators with positions $x_k \approx x$ and $|z(x,t)| < 1$ are referred to as *incoherent*.

For any f given by (14) it holds

$$z(x,t) = \int_0^{2\pi} f(\theta, y, t) e^{i\theta} d\theta.$$

This formula resembles the well-known Kuramoto's order parameter [44] with the only difference that $|z(x,t)|$ measures the synchronization of oscillators around point x rather than the global synchronization of all oscillators, therefore we call function z the *local order parameter*. Note the concept of local mean filed is consistent with Eq. (12). Indeed, Eq. (12) defines a smooth dynamical system on the Banach space $C_{\rm per}([-\pi,\pi];\mathbb{C})$. Moreover next lemma shows if we take an initial data z_0 such that $\|z_0\|_0 \le 1$ and trace its evolution according to Eq. (12) then at every time moment t we get $|z(x,t)| \le 1$.

Lemma 2 *Eq. (12) has an invariant set of the form*

$$U := \{z \in C_{\rm per}([-\pi,\pi];\mathbb{C}) \ : \ \|z\|_0 \le 1\}.$$

Proof: The complex conjugate of Eq. (12) reads

$$\frac{d\overline{z}}{dt} = -i\omega\overline{z}(x,t) + \frac{1}{2}e^{i\alpha}\mathcal{G}\overline{z} - \frac{1}{2}e^{-i\alpha}\overline{z}^2(x,t)\mathcal{G}z,$$

hence

$$\begin{aligned}\frac{d|z|^2}{dt} &= z\frac{d\overline{z}}{dt} + \overline{z}\frac{dz}{dt} = \frac{1-|z|^2}{2}\left(e^{i\alpha}z\mathcal{G}\overline{z} + e^{-i\alpha}\overline{z}\mathcal{G}z\right)\\ &= \left(1-|z|^2\right)\mathrm{Re}\left(e^{i\alpha}z\mathcal{G}\overline{z}\right).\end{aligned}$$

Taking into account that $z(x,t)$ is a continuous function of its arguments, for any fixed $x \in [-\pi,\pi]$ we get either $|z(x,t)| = 1$ for all $t \in \mathbb{R}$, or $|z(x,t)| \neq 1$ for all $t \in \mathbb{R}$. This implies the invariance of set U. •

2.3 Standing wave solutions and self-consistency equation

For particular examples of coherence-incoherence patterns considered in [19, 20] it was shown that they have periodic orbit counterparts lying in the Ott-Antonsen manifold. Assuming this correspondence as general conjecture, we develop a strategy for analysis of periodic solutions of Eq. (12).

We remark that Eq. (12) has two continuous symmetries. It is equivariant with respect to:

- spatial translations $z(x,t) \mapsto z(x+s,t), \quad s \in \mathbb{R}$,
- and complex phase shifts $z(x,t) \mapsto e^{i\varphi} z(x,t), \quad \varphi \in \mathbb{R}$.

Moreover, since coupling function G is even, the equation is also symmetric with respect to

- spatial reflections $z(x,t) \mapsto z(-x,t)$.

These symmetries suggest us to seek periodic solutions of Eq. (12) in the following form

$$z(x,t) = a(x)e^{i\Omega t}, \tag{15}$$

where $\Omega \in \mathbb{R}$ is a *collective frequency*, and $a \in C_{\mathrm{per}}([-\pi,\pi];\mathbb{C})$ is a *spatial profile*. In accordance with the probabilistic interpretation of local order parameter z, we have to ensure that $|a(x)| \leq 1$ for all $x \in [-\pi,\pi]$. Then, we refer to points $x \in [-\pi,\pi]$ with $|a(x)| = 1$ and $|a(x)| < 1$ as to the *coherent* and *incoherent regions*, respectively. In such a way we divide all the solutions described by ansatz (15) into three groups:

Name of solution	Description
Coherent (or phase-locked) state	$\lvert a(x)\rvert = 1$ for all $x \in [-\pi,\pi]$
Incoherent state	$\lvert a(x)\rvert < 1$ for all $x \in [-\pi,\pi]$
Coherence-incoherence pattern	Both coherent and incoherent regions are non-empty

For coherent and incoherent states, we also distinguish *spatially uniform* (if $a(x)$ is constant) and *spatially modulated* (otherwise) forms of these states. Finally, we call trivial solution $z \equiv 0$ the *completely incoherent* state.

Substituting ansatz (15) into Eq. (12) we obtain a self-consistency equation

$$e^{i\alpha}a^2(x)\mathcal{G}\overline{a} - 2i(\omega-\Omega)a(x) - e^{-i\alpha}\mathcal{G}a = 0. \tag{16}$$

To clarify its nature we perform a series of transformations. Assuming that $\Omega \neq \omega$ we define a new unknown function

$$w(x) := (\omega-\Omega)^{-1}\left(\mathcal{G}a\right)(x), \tag{17}$$

which is an analog of the *local mean field* in [12]. Then we rewrite Eq. (16) in the following form

$$e^{-i\beta}\overline{w}(x)a^2(x) - 2a(x) + e^{i\beta}w(x) = 0, \tag{18}$$

where

$$\beta := \frac{\pi}{2} - \alpha. \tag{19}$$

For fixed $w(x)$, quadratic Eq. (18) has two solution branches

$$a_{\pm}(x) = \begin{cases} \dfrac{1 \pm \sqrt{1-|w(x)|^2}}{e^{-i\beta}\overline{w}(x)} & \text{for} \quad |w(x)| < 1, \\ \dfrac{1 \pm i\sqrt{|w(x)|^2-1}}{e^{-i\beta}\overline{w}(x)} & \text{for} \quad |w(x)| \geq 1, \end{cases} \tag{20}$$

which satisfy $|a_-(x)||a_+(x)| = 1$. If $|w(x)| < 1$ then it holds $|a_-(x)| < 1$ and $|a_+(x)| > 1$. Therefore in order to be consistent with the requirement $|a(x)| \leq 1$ we have to assume $a(x) = a_-(x)$. On the other hand, if $|w(x)| \geq 1$ we get $|a_-(x)| = |a_+(x)| = 1$, and both branches $a_-(x)$ and $a_+(x)$ are appropriate candidates for $a(x)$. Taking into account the above definition of coherent and incoherent regions, we characterize them with the help of function $w(x)$ as follows

$$\begin{aligned} S_{\text{coh}}(w) &:= \{x \in [-\pi, \pi] \,:\, |w(x)| \geq 1\}, \\ S_{\text{incoh}}(w) &:= \{x \in [-\pi, \pi] \,:\, |w(x)| < 1\}. \end{aligned} \tag{21}$$

Now, to make definition (17) consistent with Eq. (18) we have to assume that function $w(x)$ satisfies

$$\begin{aligned} w(x) &= (\omega - \Omega)^{-1} \left(\int\limits_{S_{\text{incoh}}(w)} G(x-y) \frac{1 - \sqrt{1-|w(y)|^2}}{e^{-i\beta}\overline{w}(y)} dy \right. \\ &\left. + \int\limits_{S_{\text{coh}}(w)} G(x-y) \frac{1 \pm i\sqrt{|w(y)|^2-1}}{e^{-i\beta}\overline{w}(y)} dy \right). \end{aligned} \tag{22}$$

Note that depending on the choice $a(x) = a_-(x)$ or $a(x) = a_+(x)$ in the coherent region $S_{\text{coh}}(w)$, we obtain two different equations (22)$_-$ and (22)$_+$. Defining a complex parameter

$$\mu := (\omega - \Omega)e^{-i\beta} = (\omega - \Omega)e^{-i(\pi/2-\alpha)} \tag{23}$$

and a complex-valued function

$$h(s) := \begin{cases} \dfrac{1-\sqrt{1-s}}{s} = \dfrac{1}{1+\sqrt{1-s}} & \text{for} \quad 0 \leq s < 1, \\ \dfrac{1-i\sqrt{s-1}}{s} = \dfrac{1}{1+i\sqrt{s-1}} & \text{for} \quad s \geq 1, \end{cases} \tag{24}$$

we rewrite Eqs. $(22)_-$ and $(22)_+$ as

$$\mu w(x) = \int_{-\pi}^{\pi} G(x-y) h\left(|w(y)|^2\right) w(y) dy, \tag{25}$$

and

$$\mu w(x) = \int_{-\pi}^{\pi} G(x-y) \overline{h}\left(|w(y)|^2\right) w(y) dy, \tag{26}$$

respectively. These Eqs. (25) and (26) are nonlinear eigenvalue problems (NEVP) to be solved with respect to $\mu \in \mathbb{C}$ and $w \in C_{\mathrm{per}}([-\pi,\pi];\mathbb{C})$ simultaneously. Obviously they are not independent: Every solution (μ, w) of Eq. (25) gives a solution $(\overline{\mu}, \overline{w})$ of Eq. (26) and vice versa.

The way we derived Eqs. (25) and (26) implies that every solution (μ, w) of Eq. (25) or Eq. (26) corresponds to a solution of Eq. (12), which is given by ansatz (15) with collective frequency Ω and spatial profile $a(x)$ determined by formulas (20) and (23). Note that for any $\mu \neq 0$ identity (23) has two equivalent forms

$$(\omega - \Omega) e^{-i\beta} = \mu = |\mu| e^{i \arg \mu} = -|\mu| e^{i(\pi + \arg \mu)},$$

and hence two possible choices of (Ω, β). This fact together with the relationship between solutions of Eqs. (25) and (26) results in the following

Proposition 1 *Suppose that pair* $(\mu, w) \in \mathbb{C} \times C_{\mathrm{per}}([-\pi,\pi];\mathbb{C})$ *solves Eq. (25), then Eq. (12) has four solutions of the form (15):*

$$\begin{aligned}
&(i) \quad \Omega = \omega - |\mu|, \quad a(x) = h\left(|w(x)|^2\right) w(x) \qquad \textit{for} \quad \beta = -\arg \mu, \\
&(ii) \quad \Omega = \omega + |\mu|, \quad a(x) = h\left(|w(x)|^2\right) w(x) \qquad \textit{for} \quad \beta = -\pi - \arg \mu, \\
&(iii) \quad \Omega = \omega - |\mu|, \quad a(x) = \overline{h}\left(|w(x)|^2\right) \overline{w}(x) \qquad \textit{for} \quad \beta = \arg \mu, \\
&(iv) \quad \Omega = \omega + |\mu|, \quad a(x) = \overline{h}\left(|w(x)|^2\right) \overline{w}(x) \qquad \textit{for} \quad \beta = \pi + \arg \mu.
\end{aligned}$$

Remark 2 *If pair* (μ, w) *is real, e.g.* $\mu \in \mathbb{R}$ *and* $w \in C_{\mathrm{per}}([-\pi,\pi];\mathbb{R})$*, then solutions defined in lines (iii) and (iv) are identical to those from lines (i) and (ii), respectively.*

Proposition 1 claims that every solution of Eq. (25) or (26) corresponds to some standing wave solution of Eq. (12). But the opposite, in general, is not true. Indeed, deriving Eq. (22) we assumed that either $a(x) = a_-(x)$ or $a(x) = a_+(x)$ uniformly for all $x \in S_{\mathrm{coh}}(w)$. Now suppose that the set $S_{\mathrm{coh}}(w)$ consists of several disjoint intervals. Then, in each of those intervals we may select between branches $a_-(x)$ and $a_+(x)$ independently, without violating the continuity of the resulting profile $a(x)$. Every such choice produces a different, more complicated form of Eq. (22). Solving it we obtain standing waves, which are described neither by Eq. (25) nor by Eq. (26). Fortunately, these 'exotic' standing wave solutions turn out to be unstable, see Proposition 2. Therefore, we may expect that solving Eq. (25) and applying Proposition 1 we find all solutions relevant to observable states of system (2)–(3).

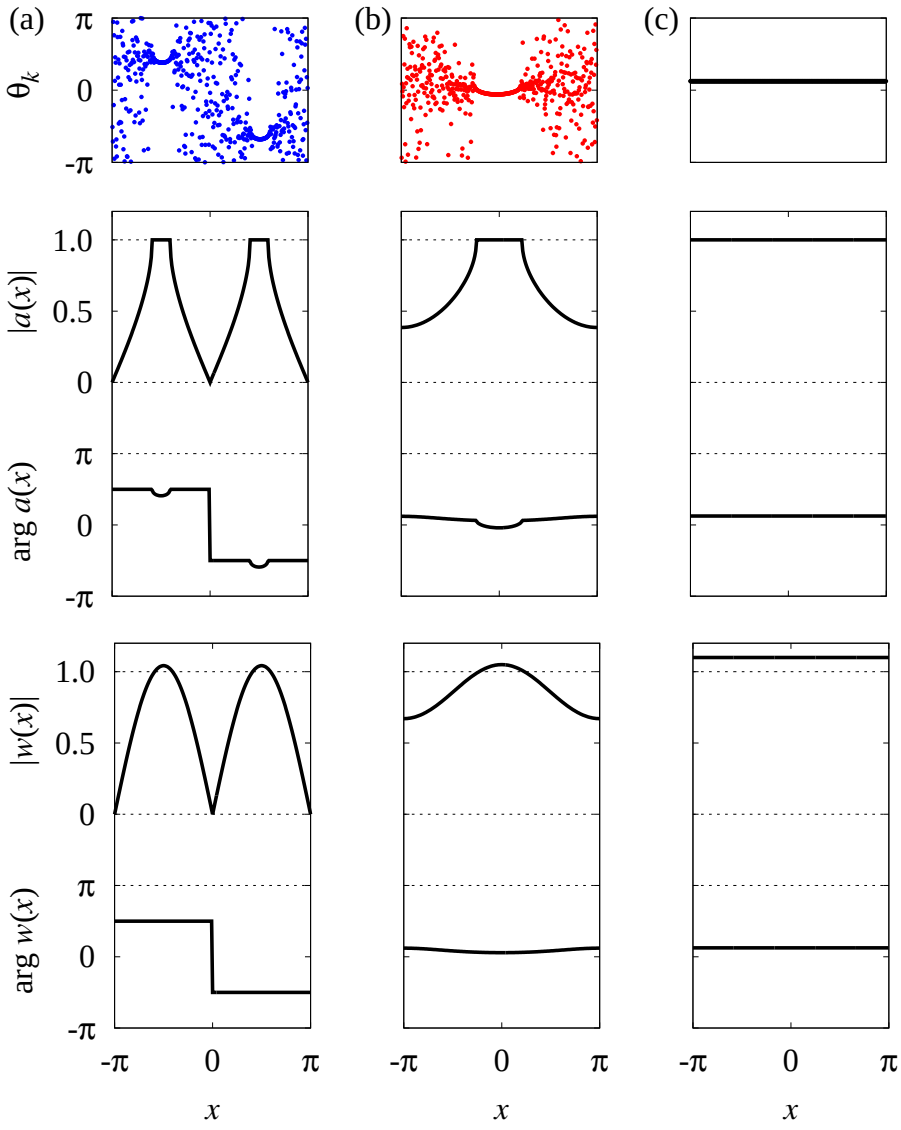

Figure 3: Continuum limit representation of two coherence-incoherence patterns (a) and (b), and completely synchronized state (c). Top panels display snapshots of the states found in numerical simulation of system (2)–(3) with $N = 500$, $\omega = 0$, $\alpha = \pi/2 - 0.1$, and cosine coupling (4) where $A = 0.9$. Other panels beneath display the amplitude $a(x)$ of corresponding standing wave, and the corresponding complex profile $w(x) = (\omega - \Omega)^{-1}(\mathcal{G}w)(x)$.

Now we can outline our program for bifurcation analysis of coherence-incoherence patterns in system (2)–(3). Fig. 3 illustrates our main tools. Instead of looking for generalized solutions of continuum limit equation (10)–(11) we look for continuous functions $z(x,t)$ solving Eq. (12). We focus on standing wave solutions described by ansatz (15) with $a \in C_{\mathrm{per}}([-\pi,\pi];\mathbb{R})$ and $\Omega \in \mathbb{R}$. The coherent and incoherent regions of such waves are fixed by conditions $|a(x)| = 1$ and $|a(x)| < 1$, respectively. Therefore spatial amplitude a is usually continuous but not smooth. Replacing Eq. (16) by Eq. (25) we typically get a smooth unknown function w such that coherent and incoherent regions are determined by conditions $|w(x)| \geq 1$ and $|w(x)| < 1$, respectively. In the next section we will try to characterize complete solution set of Eq. (25). Then applying Proposition 1 we transform each of found solutions (μ, w) into standing waves (15). Finally performing stability analysis of these waves with respect to Eq. (12) we will select really observable coherence-incoherence patterns.

3 Nonlinear eigenvalue problem

Defining a nonlinear substitution operator

$$\mathcal{H} : C_{\mathrm{per}}([-\pi,\pi];\mathbb{C}) \to C_{\mathrm{per}}([-\pi,\pi];\mathbb{C}), \qquad \mathcal{H}(w) := h\left(|w|^2\right) w, \tag{27}$$

where h is given by (24), and recalling that $\mathcal{G}$ denotes the integral convolution operator (13), we rewrite Eq. (25) in the abstract form

$$\mathcal{F}(\mu, w) := \mu w - \mathcal{G}\mathcal{H}(w) = 0. \tag{28}$$

This is a nonlinear eigenvalue problem to be solved with respect to pair of unknowns $(\mu, w) \in \mathbb{C} \times C_{\mathrm{per}}([-\pi,\pi];\mathbb{C})$. Its infinite-dimensional nonlinearity $\mathcal{G}\mathcal{H}(w)$ has comparatively simple mathematical nature since for coupling function G relevant to present study, corresponding operator $\mathcal{G}$ is usually compact in $C_{\mathrm{per}}([-\pi,\pi];\mathbb{C})$ or even in $C^1_{\mathrm{per}}([-\pi,\pi];\mathbb{C})$. However, NEVP (28) inherits all continuous and discrete symmetries of Eq. (12), therefore its analysis requires new approaches going beyond the classical paradigm of NEVP formulated by M. A. Krasnoselskii [45] and P. H. Rabinowitz [46].

Above we have seen that typical dynamical regimes observed in large N system (2)–(3) can be described as standing wave solutions of Eq. (12). In order to find such periodic solutions we use NEVP (28) and the correspondence between its solutions and standing waves of Eq. (12) given by Proposition 1. In Section 3.1, we address some auxiliary questions concerned with Fourier representation of integral operator $\mathcal{G}$ and differentiability of substitution operator $\mathcal{H}$. Then, in Section 3.2 we show that in general case solution set of NEVP (28) is locally organized as a curve (modulo the symmetry group action) in the Banach space $\mathbb{C} \times C_{\mathrm{per}}([-\pi,\pi];\mathbb{C})$. Some explicitly known solutions of NEVP (28) are described in Section 3.3. These solutions are counterparts of completely synchronized and twisted solutions in original system (2)–(3). In Section 3.4 we analyze primary solution branches bifurcating from the trivial solution $w = 0$. Then, in Section 3.5 we describe a sequence of secondary solution branches which appear from the primary branch of spatially uniform solutions. At the end we present two illustrative examples for piecewise-constant and cosine coupling.

3.1 Auxiliary facts about operators $\mathcal{G}$ and $\mathcal{H}$

Generalizing examples from [12, 14, 23], let us suppose that coupling function G satisfies the following conditions

- it is piecewise-smooth, that means it is C^1-smooth on a finite number of disjoint intervals, obtained as a partition of the interval $[-\pi, \pi]$,
- it is non-constant,
- it is even, i.e. $G(-x) = G(x)$,
- it is 2π-periodic.

These conditions in particular imply that G has an absolutely converging Fourier series

$$G(x) = \sum_{k=-\infty}^{\infty} g_k e^{ikx}, \quad \text{with coefficients} \quad g_k = \frac{1}{2\pi} \int_{-\pi}^{\pi} G(x) e^{-ikx}\, dx. \tag{29}$$

Since G is even, all g_k's are real and it holds $g_k = g_{-k}$. Formula (29) also implies that operator $\mathcal{G}$ is diagonizable in the Fourier space and can be represented in the form

$$(\mathcal{G}w)(x) = \sum_{k=-\infty}^{\infty} g_k e^{ikx} \int_{-\pi}^{\pi} e^{-iky} w(y) dy.$$

Applying this we easily get

$$\left(\mathcal{G}e^{ikx}\right)(x) = 2\pi g_k e^{ikx} \quad \text{for any} \quad k \in \mathbb{Z}. \tag{30}$$

Moreover, using identity $g_k = g_{-k}$ it is easy to verify that for any integer $k \geq 0$ and any function $u \in C_{\mathrm{per}}([-\pi, \pi]; \mathbb{C})$ it holds

$$\begin{aligned} \langle \cos(kx), \mathcal{G}u \rangle &= 2\pi g_k \langle \cos(kx), u \rangle, \\ \langle \sin(kx), \mathcal{G}u \rangle &= 2\pi g_k \langle \sin(kx), u \rangle, \end{aligned}$$

where inner product $\langle \cdot, \cdot \rangle$ is defined by (7).

Presence of integral operator $\mathcal{G}$ usually makes Eq. (28) infinite-dimensional. However, performing its numerical evaluation we often can replace this operator with a finite-rank approximation obtained via truncating the Fourier series (29). For example, if we define

$$(\mathcal{G}_K w)(x) := \int_{-\pi}^{\pi} G_K(x - y) w(y) dy, \quad K = 1, 2, \ldots,$$

where

$$G_K(x) = \sum_{k=-K}^{K} g_k e^{ikx} = g_0 + \sum_{k=1}^{K} 2 g_k \cos(kx), \tag{31}$$

then using the Hölder inequality and the L^2-convergence of Fourier series (29) we easily obtain

$$\lim_{K\to\infty} \|\mathcal{G} - \mathcal{G}_K\| = 0, \tag{32}$$

where convergence takes place in the strong operator norm of Banach space $C_{\rm per}([-\pi,\pi];\mathbb{C})$.

Infinite-dimensional range of operator $\mathcal{G}$ is not the only difficulty concerned with NEVP (28). In principle, we could expect that local structure of its solution set can be revealed via the Implicit Function Theorem. But, for this we must know the derivative

$$\partial_w \mathcal{F}(\mu, w) = \mu\mathcal{I} - \mathcal{G}\mathcal{H}'(w), \tag{33}$$

which is not correctly defined on $C_{\rm per}([-\pi,\pi];\mathbb{C})$ because definition of operator $\mathcal{H}$ contains the absolute value $|w|$. To avoid this problem let us identify Banach space $C_{\rm per}([-\pi,\pi];\mathbb{C})$ with its real counterpart $C_{\rm per}([-\pi,\pi];\mathbb{R}^2)$. In other words, let us consider Eq. (28) as a system of two equations for real and imaginary parts separately. After such a reformulation, we easily calculate

$$\begin{aligned} \mathcal{H}'(w)v &= \frac{d}{ds}\Big[h(|w+sv|^2)(w+sv)\Big]\Big|_{s=0} \\ &= h(|w|^2)v + 2wh'(|w|^2)\,\mathrm{Re}(\overline{w}v), \end{aligned} \tag{34}$$

where

$$h'(s) = \begin{cases} \dfrac{1}{2(1+\sqrt{1-s})^2\sqrt{1-s}} & \text{for} \quad 0 \le s < 1, \\ -\dfrac{i}{2(1+i\sqrt{s-1})^2\sqrt{s-1}} & \text{for} \quad s \ge 1. \end{cases} \tag{35}$$

Note that derivative $h'(s)$ has a singularity at $s = 1$, therefore operator $\mathcal{H}$ still fails to be differentable on the whole space $C_{\rm per}([-\pi,\pi];\mathbb{R}^2)$. On the other hand, within the ball

$$\Big\{ w \in C_{\rm per}([-\pi,\pi];\mathbb{R}^2) \;:\; |w(x)| < 1 \quad \text{for all} \quad x \in [-\pi,\pi] \Big\}$$

it has derivatives of arbitrary order. In particular,

$$\begin{aligned} \mathcal{H}''(w)v^2 &= 4vh'(|w|^2)\,\mathrm{Re}(\overline{w}v) + 2wh'(|w|^2)|v|^2 \\ &+ 4wh''(|w|^2)\,\mathrm{Re}^2(\overline{w}v), \end{aligned} \tag{36}$$

$$\begin{aligned} \mathcal{H}'''(w)v^3 &= 6h'(|w|^2)|v|^2 v + 12wh''(|w|^2)|v|^2\,\mathrm{Re}(\overline{w}v) \\ &+ 12vh''(|w|^2)\,\mathrm{Re}^2(\overline{w}v) + 8wh'''(|w|^2)\,\mathrm{Re}^3(\overline{w}v). \end{aligned} \tag{37}$$

Above we have seen that for coherence-incoherence patterns both inequalities $|w(x)| < 1$ and $|w(x)| \ge 1$ occur at different positions x. Therefore nondifferentiability of $\mathcal{H}$ is unavoidable. Fortunately this makes no problem if we take into account the smoothening effect of integral operator $\mathcal{G}$. Indeed, suppose that (μ, w) is a solution of NEVP (28), then for any piecewise-smooth coupling function G it holds $w \in C^1_{\rm per}([-\pi,\pi];\mathbb{R}^2)$. Hence, without loss of generality we may restrict NEVP (28) to the subspace of smooth functions w. After we did this, we can prove the local differentiability of product operator $\mathcal{G}\mathcal{H}$, what in most cases is enough for application of the Implicit Function Theorem.

Lemma 3 *Suppose that G is a piecewise-smooth function, then for any $w_0 \in C^1_{\rm per}([-\pi,\pi];\mathbb{R}^2)$ satisfying*

$$\varkappa(w_0) := \inf_{x\in[-\pi,\pi]} \left(\Big| |w_0(x)| - 1 \Big| + \left| \frac{d|w_0(x)|^2}{dx} \right| \right) > 0, \tag{38}$$

there exists $\delta > 0$ such that operator $\mathcal{GH}(w)$ is differentiable at any $w \in C^1_{\rm per}([-\pi,\pi];\mathbb{R}^2)$ within the ball $\|w - w_0\|_1 < \delta$.

Proof: Due to assumption (38) equation $|w_0(x)| = 1$ has at most a finite number, say L, of simple roots $\xi^0_1, \ldots, \xi^0_L \in [-\pi,\pi]$. Moreover, for each ξ^0_k there exists $\delta_k > 0$ such that

$$\Big| |w_0(x)| - 1 \Big| \geq \frac{\varkappa}{2} |x - \xi^0_k| \qquad \text{for all} \qquad |x - \xi^0_k| < \delta_k.$$

Hence, choosing $\delta > 0$ small enough, we ensure that for all $w \in C^1_{\rm per}([-\pi,\pi];\mathbb{R}^2)$ within the ball $\|w - w_0\|_1 < \delta$ the following properties are fulfilled:

(i) The equation $|w(x)| = 1$ has exactly L simple roots $\xi_1(w), \ldots, \xi_L(w)$, which continuously depend on w, and $\xi_k(w_0) = \xi^0_k$, $k = 1, \ldots, L$.

(ii) For all $|x - \xi_k(w)| < \delta_k/2$ it holds

$$\Big| |w(x)| - 1 \Big| \geq \frac{\varkappa}{4} \, |x - \xi_k(w)| \, .$$

The latter inequality together with formula (35) imply

$$\Big| f' \left(|w(x)|^2 \right) \Big| \leq C_0 \Big| |w(x)| - 1 \Big|^{-1/2} \leq \frac{4C_0}{\varkappa} |x - \xi_k(w)|^{-1/2}$$

for all $|x - \xi_k(w)| < \delta_k/2$, where $C_0(\delta) > 0$ is a constant independent of w. Now, from formula (34) we easily see that the substitution operator

$$\mathcal{H} : C^1_{\rm per}([-\pi,\pi];\mathbb{R}^2) \to L^1_{\rm per}([-\pi,\pi];\mathbb{C})$$

is differentiable at any $w \in C^1_{\rm per}([-\pi,\pi];\mathbb{R}^2)$ within the ball $\|w - w_0\|_1 < \delta$. On the other hand, for any smooth coupling function G the corresponding convolution operator $\mathcal{G}$ is a bounded linear operator from $L^1_{\rm per}([-\pi,\pi];\mathbb{C})$ into $C^1_{\rm per}([-\pi,\pi];\mathbb{R}^2)$. Hence, the assertion of lemma is proved. •

Roughly speaking, Lemma 3 claims that product operator $\mathcal{GH}$ is differentiable everywhere in $C^1_{\rm per}([-\pi,\pi];\mathbb{R}^2)$ except of the zero measure set

$$\Sigma_0 := \left\{ w \in C^1_{\rm per}([-\pi,\pi];\mathbb{R}^2) \ : \ \varkappa(w) = 0 \right\}. \tag{39}$$

Thus we may expect that local behavior of the solution set of NEVP (28) is generically determined by properties of the linearized operator $\partial_w \mathcal{F}(\mu, w)$. However, a particular singular behaviour may happen if w passes through the set Σ_0.

3.2 Local structure of the solution set of NEVP

Suppose that we know a particular solution (μ_0, w_0) of NEVP (28). Then, what can we say about the local structure of its solution set close to this point? Below we provide a constructive answer on this question.

We assume that $\mu_0 \neq 0$ and $w_0 \neq 0$ (the case of trivial solution $w_0 = 0$ is considered in Section 3.4), then we choose a nonvanishing function $\psi \in C^1_{\rm per}([-\pi, \pi]; \mathbb{R})$ such that

$$p_0 = \left| \frac{\langle \psi, w_0 \rangle}{\langle \psi, \psi \rangle} \right| \neq 0 \tag{40}$$

(such ψ can always be found for example among the Fourier harmonics $\cos(kx)$ and $\sin(kx)$, $k = 0, 1, \ldots$). Let us define a Fourier projection of the form

$$\mathcal{P}_\psi w := \frac{\langle \psi, w \rangle}{\langle \psi, \psi \rangle} \psi,$$

with the kernel

$$\Pi_\psi := \left\{ w \in C^1_{\rm per}([-\pi, \pi]; \mathbb{R}^2) \ : \ \mathcal{P}_\psi w = 0 \right\}.$$

Applying operators $\mathcal{P}_\psi$ and $\mathcal{I} - \mathcal{P}_\psi$ to Eq. (28) and omitting the non-zero factor $\psi / \langle \psi, \psi \rangle$ in the former result, we rewrite Eq. (28) as an equivalent system

$$\mu \langle \psi, w \rangle = \langle \psi, \mathcal{G}\mathcal{H}(w) \rangle, \tag{41}$$

$$\mu (\mathcal{I} - \mathcal{P}_\psi) w = (\mathcal{I} - \mathcal{P}_\psi) \mathcal{G}\mathcal{H}(w). \tag{42}$$

Then taking into account assumption (40), we divide Eq. (42) by Eq. (41) and obtain

$$\frac{(\mathcal{I} - \mathcal{P}_\psi) w}{\langle \psi, w \rangle} = \frac{(\mathcal{I} - \mathcal{P}_\psi) \mathcal{G}\mathcal{H}(w)}{\langle \psi, \mathcal{G}\mathcal{H}(w) \rangle}. \tag{43}$$

System of two equations (41) and (43) is equivalent (at least in a vicinity of point (μ_0, w_0)) to original Eq. (28). On the other hand, Eq. (43) is decoupled from Eq. (41) and does not contain complex unknown μ. In order to solve Eq. (43) we represent w in the form

$$w = v + p\psi, \quad \text{where} \quad v \in \Pi_\psi \quad \text{and} \quad p \in \mathbb{R}_+. \tag{44}$$

Such a decomposition is uniquely determined due to the phase-shift symmetry of original Eq. (28). Substituting ansatz (44) into Eq. (43) we get

$$v = \frac{(\mathcal{I} - \mathcal{P}_\psi) \mathcal{G}\mathcal{H}(v + p\psi)}{\langle \psi, \mathcal{G}\mathcal{H}(v + p\psi) \rangle} \langle \psi, \psi \rangle p =: \mathcal{E}_\psi(v, p). \tag{45}$$

This is an equation to be solved with respect to $v \in \Pi_\psi$, for a given $p \in \mathbb{R}_+$ close to p_0. As soon as Eq. (45) is solved, formulas (41) and (44) determine the corresponding pair (μ, w). Hence, we have established a one-to-one correspondence between solutions of Eq. (45) and solutions of Eq. (28) which obey the phase-pinning condition $\langle \psi, w \rangle = |\langle \psi, w \rangle|$.

Remark if ψ is not identically constant, then Eq. (45) generically does not inherit continuous symmetries of Eq. (28). That means, Eq. (45) is not equivariant either with respect to spatial translations, or with respect to phase-shifts (the latter symmetry has gone after we had fixed p to be real). This observation clarifies the true nature of Eq. (28) and opens the way for computing its approximate solutions with the help of classical numerical schemes. Indeed, suppose that for a given $w_0 \neq 0$ there exists bounded derivative $\mathcal{GH}'(w_0)$, then for appropriate choice of ψ satisfying (40), we can linearize reduced Eq. (45) around v_0, where v_0 is uniquely determined from the decomposition $w_0 = v_0 + p_0\psi$ with $v_0 \in \Pi_\psi$ and $p_0 \in \mathbb{R}_+$. Corresponding linearized operator $\mathcal{I} - \partial_v\mathcal{E}_\psi(v_0, p_0)$ is Fredholm of index zero (as a sum of invertible $\mathcal{I}$ plus compact operator), and hence it has at most a finite dimensional kernel. Therefore solving Eq. (45) we generically meet one of the following three situations:

- the derivative $\mathcal{GH}'(w_0)$ is well-defined and $\ker(\mathcal{I} - \partial_v\mathcal{E}_\psi(v_0, p_0)) = \{0\}$, then there exists a unique, locally determined solution curve $v = v(p)$ such that $v(p_0) = v_0$;
- the derivative $\mathcal{GH}'(w_0)$ is well-defined but $\ker(\mathcal{I} - \partial_v\mathcal{E}_\psi(v_0, p_0)) \neq \{0\}$, then point (v_0, p_0) is a bifurcation point of Eq. (45) with finite codimension;
- operator $\mathcal{GH}$ is not differentiable at w_0, then analysis gets more involved but it is possbile to demonstrate that close to point w_0 we typically observe a particular transformation of coherence-incoherence pattern when the pattern gets/loses a coherence region.

If operator $\mathcal{GH}(w)$ is differentiable at w_0, then reduced Eq. (45) can be solved locally by applying a variant of Galerkin's method. For the sake of completeness we recall general framework of this approach. Suppose that we chose ψ for decomposition (44) and look for solution v of Eq. (45) in a Banach space $X \subset \Pi_\psi$ which has an orthogonal basis $\{v_k\}$. This solution can be found approximately as a sum of the form

$$v \approx \sum_{k=1}^{K} \hat{v}_k v_k, \tag{46}$$

where coefficients $\hat{v}_k \in \mathbb{C}$ are determined from the projected system

$$\langle v_n, v_n\rangle \hat{v}_n = \left\langle v_n, \mathcal{E}_\psi\left(\sum_{k=1}^{K} \hat{v}_k v_k, p\right)\right\rangle, \quad n = 1, \ldots, K. \tag{47}$$

In all cases relevant to present study, operator $\mathcal{E}_\psi(v, p)$ is compact on X. Therefore for sufficiently large integer K, sum (46) approximates all exact solutions of Eq. (45) that exist in a small vicinity of $v_0 = w_0 - \mathcal{P}_\psi w_0$. More precisely, solving system (47) we distinguish all local bifurcations occurring in the non-reduced Eq. (28).

But what shall we do with singular points (μ_0, w_0) where operator $\mathcal{GH}$ is not differentiable? In principle, we may look for appropriate substitution revealing bifurcation scenario there. However, we choose another, simpler way. Let us define $\mathcal{H}_\epsilon(w) = h_\epsilon(|w|)w$ where

$$h_\epsilon(s) = \frac{1}{1 + \sqrt{1 - s + i\epsilon}} \quad \text{and} \quad \epsilon > 0.$$

For any fixed $\epsilon > 0$ operator $\mathcal{H}_\epsilon(w)$ is differentiable in $C_{\rm per}([-\pi,\pi];\mathbb{R}^2)$ and satisfies

$$\lim_{\epsilon\to+0}\mathcal{H}_\epsilon(w) = \mathcal{H}(w).$$

Hence, if in Eqs. (46) we replace operator $\mathcal{GH}$ by its regularized analog $\mathcal{GH}_\epsilon$ and solve the resulting system, then we obtain an ϵ-dependent solution curve which passes through the 'dangerous' vicinity of point (μ_0, w_0). Now restoring operator $\mathcal{GH}$ in Eqs. (46) and taking the ϵ-dependent solution as initial guess for the Newton's scheme, we can calculate two parts of true solution curve (for $\epsilon \to +0$) approaching singular point from two different directions. Typically we obtain a solution curve that bends at the singular point, see Figs. 5 and 6, therefore we refer to this singularity as to the *bending bifurcation* point. Such behaviour may look strange, but if we recall that solving Eq. (18) we obtained two complex-conjugate equations (25) and (26) it becomes clear that bending bifurcation is nothing else but a reminiscence of complex fold.

3.3 Explicit solutions of NEVP

Some solutions of Eq. (28) can be found explicitly. They have a form

$$w(x) = pe^{ikx} \quad \text{where} \quad k\in\mathbb{Z} \quad \text{and} \quad p\in(0,\infty). \tag{48}$$

Indeed, substituting ansatz (48) into Eq. (28) and taking into account identity (30) we get

$$\left(\mu - 2\pi g_k h(p^2)\right) pe^{ikx} = 0$$

where function h was defined above, see (24). Hence for every $k\in\mathbb{Z}$ formula (48) determines a nontrivial solution of Eq. (28), provided

$$\mu = 2\pi g_k h(p^2). \tag{49}$$

Applying definition of function h we rewrite this equation more explicitly distinguishing two particular cases:

$$p<1 \quad \text{and} \quad \mu = \frac{2\pi g_k}{1+\sqrt{1-p^2}}, \tag{50}$$

$$p\geq 1 \quad \text{and} \quad \mu = \frac{2\pi g_k}{1-i\sqrt{p^2-1}}. \tag{51}$$

In the former case, μ is real, see Fig. 4. Therefore definition (23) implies that all solutions (48) with $p\in(0,1)$ correspond to two particular phase lags only, $\alpha = \pi/2$ and $\alpha = -\pi/2$. In contrary, for $p\geq 1$ formulas (48) and (51) connect different values p with different values α. Moreover according to the local order parameter interpretation, see Section 2, we may consider solutions (48) with $p\geq 1$ as counterparts of the completely synchronized state (for $k=0$) or twisted states (for $k\neq 0$) observed in original system (2)–(3).

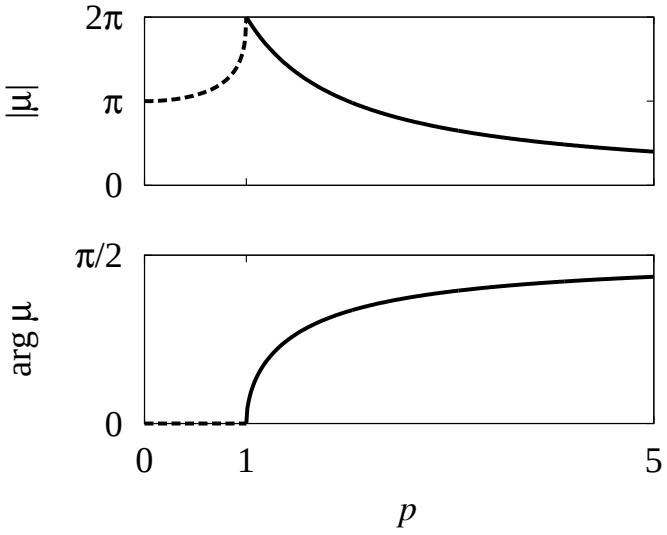

Figure 4: Explicit solution of NEVP (28) determined by Eq. (50) (dashed line) and Eq. (51) (solid line) for $g_k = 1$.

3.4 Primary solution branches

We start off with a more systematic approach for describing the solution set of NEVP (28). To this end, we linearize this equation around its trivial solution $w = 0$ and look for such values μ where conditions of the Implicit Function Theorem are violated. Applying formulas (33) and (34) we obtain

$$\partial_w \mathcal{F}(\mu, 0) = \mu \mathcal{I} - \mathcal{G}\mathcal{H}'(0) = \mu \mathcal{I} - \frac{1}{2}\mathcal{G}. \tag{52}$$

Spectrum of operator $\mathcal{G}$ is known explicitly, see Section 3.1, therefore we easily demonstrate that derivative $\partial_w \mathcal{F}(\mu, 0)$ is not invertible if

$$\mu = \mu_k := \pi g_k, \quad k = 0, 1, 2, \ldots. \tag{53}$$

Moreover, in generic case for each non-zero μ_k it holds

$$\ker \partial_w \mathcal{F}(\mu_k, 0) = \operatorname{span}\left\{e^{ikx}, e^{-ikx}\right\}.$$

Remark that Eq. (49) implies $2\pi g_k h(0) = \mu_k$, hence all solutions of NEVP (28) described by formula (48) bifurcate from zero exactly at critical values of operator $\partial_w \mathcal{F}(\mu, 0)$. However, there is also another sequence of primary branches bifurcating at the same values μ_k.

Lemma 4 *Suppose that g_k, $k \geq 1$, is a non-zero Fourier coefficient of G.*

Then, for all sufficiently small $\mu - \mu_k \in \mathbb{R}$ such that $(\mu - \mu_k) g_k > 0$, generically there exists a non-trivial solution of Eq. (28) with an asymptotic

$$w(x) = 4\sqrt{\frac{1}{3\pi g_k}(\mu - \mu_k)}\sin(kx) + O(|\mu - \mu_k|) \quad \textit{for} \quad \mu \to \mu_k. \tag{54}$$

Proof: We restrict Eq. (28) to its invariant subspace

$$(\mu, w) \in \mathbb{R} \times C_{\mathrm{per,odd}}([-\pi, \pi]; \mathbb{R})$$

where

$$C_{\mathrm{per,odd}}([-\pi, \pi]; \mathbb{R}) := \left\{ w \in C_{\mathrm{per}}([-\pi, \pi]; \mathbb{R}) \ : \ w(-x) = -w(x) \right\}.$$

Then derivative $\partial_w \mathcal{F}(\mu, 0)$ is degenerate at $\mu = \mu_k$ with one-dimensional kernel spanned by $\sin(kx)$. Note the latter claim is not true if some other Fourier coefficient of G coincides with g_k, but such situation is non-generic. We proceed further with a standard Lyapunov-Schmidt reduction. For this, we define $\varepsilon^2 = \mu - \mu_k > 0$ and substitute an ansatz

$$w = \varepsilon w_1 + \varepsilon^2 w_2 + \varepsilon^3 w_3 + \dots \tag{55}$$

into Eq. (28). Then expanding nonlinearity $\mathcal{GF}(w)$ with the help of asymptotic formula

$$\mathcal{GF}(w) = \frac{1}{2}\mathcal{G}w + \frac{1}{8}\mathcal{G}w^3 + O(\|w\|_0^5) \quad \text{for} \quad \|w\|_0 \to 0,$$

and collecting the same order terms, we obtain a sequence of equations determining w_k. In particular,

$$\left(\mu_k \mathcal{I} - \frac{1}{2}\mathcal{G}\right) w_1 = 0 \quad \text{and} \quad \left(\mu_k \mathcal{I} - \frac{1}{2}\mathcal{G}\right) w_2 = 0.$$

This implies $w_1(x) = p_1 \sin(kx)$ and $w_2(x) = p_2 \sin(kx)$ where real constants p_1 and p_2 are not known at this step. For the next order we get

$$\left(\mu_k \mathcal{I} - \frac{1}{2}\mathcal{G}\right) w_3 = -w_1 + \frac{1}{8}\mathcal{G}w_1^3.$$

According to the Fredholm alternative, this equation has a solution if and only if its right-hand side satisfies the solvability condition

$$\int_{-\pi}^{\pi} \sin(kx) \left(-w_1(x) + \frac{1}{8} \left(\mathcal{G}w_1^3 \right)(x) \right) dx = \pi p_1 \left(\frac{3}{16} \pi g_k p_1^2 - 1 \right) = 0.$$

For $g_k > 0$, this algebraic equation has a pair of opposite sign solutions p_1 resulting in the leading term of asymptotics (54) (in the case $g_k < 0$ we have to assume $\varepsilon^2 = -(\mu - \mu_k)$ and then to repeat all above arguments). As soon as we know the leading term, we prove the existence of corresponding solution applying the Implicit Function Theorem. •

In general case, all Fourier coefficients g_k with $k \geq 0$ are non-zero and different. Hence, Lemma 4 defines infinite number of primary branches bifurcating from the trivial solution. All these branches can be numerically continuated as explained in Section 3.2. More precisely, for each $k \in \mathbb{N}$ we choose $\psi = \sin(kx)$ and solve Galerkin's system (47) in a Banach subspace $X \subset C_{\mathrm{per}}([-\pi, \pi]; \mathbb{C})$ corresponding to the isotropy group of $\sin(kx)$. This Fourier harmonics is invariant with respect to transformations

$$w(x) \mapsto w\left(x + \frac{2\pi}{k}\right), \quad w(x) \mapsto -w(-x), \quad w\left(x + \frac{\pi}{2k}\right) \mapsto w\left(-x + \frac{\pi}{2k}\right),$$

therefore we fix X to be a subspace of $C_{\rm per}([-\pi,\pi];\mathbb{C})$ with orthogonal basis

$$\sin((2m-1)kx), \quad m=2,3,\dots.$$

Particular examples considered below reveal that all primary branches have similar qualitative behaviour. Each of them initially lies in the ball Σ_0, see definition (39), but later approaches its boundary, undergoes bending bifurcation and gives rise to a curve of coherence-incoherence patterns with equidistant coherent regions, e.g. $|w(x)|\geq 1$, emerging in the incoherent background, e.g. $|w(x)|<1$.

3.5 Secondary solution branches

Performing numerical continuation of primary branches we may encounter other (secondary) bifurcation points. For example, let us consider the simplest of explicitly known solutions (48) with $k=0$. For $p\in[0,1]$ these solutions are determined by Eq. (50) which can be rewritten in the form

$$w(x)\equiv p_0(\mu):=\left|\frac{2\pi g_0}{\mu}\right|\sqrt{\frac{\mu}{\pi g_0}-1} \quad \text{where} \quad \frac{1}{2}\leq\frac{\mu}{2\pi g_0}<1. \tag{56}$$

Applying formulas (34)–(35) we easily calculate

$$\partial_w\mathcal{F}(\mu,p_0(\mu))=\mu\mathcal{I}-\mathcal{G}\mathcal{H}'(p_0(\mu))=\mu\mathcal{I}-\frac{\mu^2}{|2\pi g_0(\mu-2\pi g_0)|}\mathcal{G}.$$

Hence critical values of $\partial_w\mathcal{F}(\mu,p_0(\mu))$ again can be found from the point spectrum of operator $\mathcal{G}$. Indeed operator $\partial_w\mathcal{F}(\mu,p_0(\mu))$ is not invertible for every $\mu\in\mathbb{R}$ which satisfies at least one of the following equations

$$\frac{|2\pi g_0(\mu-2\pi g_0)|}{\mu^2}=2\pi g_k, \quad k=1,2,\dots,$$

which are equivalent to equations

$$\frac{2\pi g_0}{\mu}\left|\frac{\mu}{2\pi g_0}-1\right|=\frac{g_k}{g_0}, \quad k=1,2,\dots. \tag{57}$$

It is easy to verify that each Eq. (57) has a unique solution $\mu/(2\pi g_0)\in[1/2,1)$ provided $g_k/g_0\in(0,1]$, and has no solution from this interval otherwise. If this solution exists, it is given by

$$\nu_k:=\frac{2\pi g_0^2}{g_0+g_k}. \tag{58}$$

Remark that $\nu_0=\pi g_0$ is identical to the bifurcation value μ_0 where primary branch of spatially uniform solutions (48), e.g. branch with $k=0$, appears from the trivial solution. Next lemma shows that all other ν_k with $k\geq 1$ are points of secondary bifurcation.

Lemma 5 *Suppose that $g_0 \neq 0$ and $g_k/g_0 \in (0,1]$ for some $k \geq 1$.*

Then for sufficiently small $\mu - \nu_k \in \mathbb{R}$ such that $(\mu-\nu_k)C_0/C_1 > 0$, generically there exists a non-trivial solution of Eq. (28) with an asymptotic

$$w(y) = p_0(\nu_k) + \sqrt{\frac{C_0}{C_1}(\mu-\nu_k)}\cos(kx) + O(|\mu-\nu_k|) \quad \textit{for} \quad \mu \to \nu_k, \tag{59}$$

where

$$\begin{aligned} C_0 &= 1 - 2\pi g_k c_2 p_0'(\nu_k), \\ C_1 &= \frac{1}{4}\pi g_k \left(c_3 + \frac{4\pi g_0 c_2^2}{\nu_k - 2\pi g_0 c_1} + \frac{2\pi g_{2k} c_2^2}{\nu_k - 2\pi g_{2k} c_1} \right), \end{aligned}$$

and

$$c_m := \mathcal{H}^{(m)}(p_0(\nu_k)) = \frac{d^k}{du^k}\left(\frac{u}{1+\sqrt{1-u^2}} \right)\Big|_{u=p_0(\nu_k)}.$$

Proof: The proof is a more technical version of that in Lemma 4. We restrict Eq. (28) to its invariant subspace

$$(\mu, w) \in \mathbb{R} \times C_{\rm per,even}([-\pi,\pi];\mathbb{R})$$

where

$$C_{\rm per,even}([-\pi,\pi];\mathbb{R}) := \left\{ w \in C_{\rm per}([-\pi,\pi];\mathbb{R}) \ : \ w(-x) = w(x) \right\}.$$

Then we denote $\varepsilon^2 = \mu - \nu_k > 0$ and look for solutions of the form

$$w = p_0(\nu_k + \varepsilon^2) + \varepsilon w_1 + \varepsilon^2 w_2 + \varepsilon^3 w_3 + \ldots.$$

This ansatz implies

$$\begin{aligned} \mu w &= (\nu_k + \varepsilon^2) w = \nu_k p_0(\nu_k) + \varepsilon \nu_k w_1 \\ &+ \varepsilon^2 \left(\nu_k w_2 + p_0(\nu_k) + \nu_k p_0'(\nu_k) \right) + \varepsilon^3 \left(\nu_k w_3 + w_1 \right) + O(\varepsilon^4) \end{aligned}$$

and

$$\begin{aligned} \mathcal{H}(p_0(\mu)+w) &= \mathcal{H}(p_0(\nu_k+\varepsilon^2)+w) = \mathcal{H}(p_0(\nu_k)) + \varepsilon \mathcal{H}'(p_0(\nu_k))w_1 \\ &+\varepsilon^2 \left(\mathcal{H}'(p_0(\nu_k))(w_2 + p_0'(\nu_k)) + \frac{1}{2}\mathcal{H}''(p_0(\nu_k))w_1^2 \right) \\ &+\varepsilon^3 \left(\mathcal{H}'(p_0(\nu_k))w_3 + \mathcal{H}''(p_0(\nu_k))w_1(w_2 + p_0'(\nu_k)) + \frac{1}{6}\mathcal{H}'''(p_0(\nu_k))w_1^3 \right) + O(\varepsilon^4). \end{aligned}$$

Thus expanding Eq. (28) with respect to small parameter ε and collecting the same order terms, we obtain equations

$$(\nu_k \mathcal{I} - c_1 \mathcal{G})\, w_1 = 0, \tag{60}$$

$$(\nu_k \mathcal{I} - c_1 \mathcal{G})\, w_2 = \frac{1}{2} c_2 \mathcal{G} w_1^2, \tag{61}$$

$$(\nu_k \mathcal{I} - c_1 \mathcal{G})\, w_3 = -w_1 + c_2 \mathcal{G} w_1 (w_2 + p_0'(\nu_k)) + \frac{1}{6} a_3 \mathcal{G} w_1^3. \tag{62}$$

Note that to simplify the right-hand sides of Eqs. (61)–(62) we used identity $\mathcal{F}(\mu, p_0(\mu)) = 0$ and its full derivative with respect to μ.

Eqs. (60) and (61) can be solved explicitly. Thus we obtain

$$w_1(x) = p_1 \cos(kx),$$
$$w_2(x) = p_2 \cos(kx) + \frac{1}{4} c_2 p_1^2 \left(\frac{2\pi g_0}{\nu_k - 2\pi g_0 c_1} + \frac{2\pi c_{2k}}{\nu_k - 2\pi g_{2k} c_1} \cos(2kx) \right),$$

where $p_1, p_2 \in \mathbb{R}$ are not known at this step. Remark that in generic case denominators in formula for w_2 do not vanish. Now writing solvability condition for Eq. (62) and inserting there expressions for w_1 and w_2, we get

$$\int_{-\pi}^{\pi} \cos(kx) \left(-w_1(x) + c_2 \left(\mathcal{G} w_1 (w_2 + p_0'(\nu_k)) \right)(x) + \frac{1}{6} c_3 \left(\mathcal{G} w_1^3 \right)(x) \right) dx$$
$$= \pi p_1 (C_1 p_1^2 - C_0) = 0.$$

For $C_0/C_1 > 0$ this algebraic equation has a pair of nontrivial solutions p_1 (for $C_0/C_1 < 0$ one has to repeat all arguments with $\varepsilon^2 = -(\mu - \nu_k)$). Hence applying the Implicit Function Theorem we can justify asymptotics (59). •

Similar to Section 3.4, we may suggest that in general case Lemma 5 defines infinite number of secondary solution branches. However, this is only a part of the story. In fact, appearance of secondary branches is more sensitive to the signs and absolute values of Fourier coefficients g_k. In particular, bifurcation corresponding to g_k occurs only if $g_k/g_0 \in (0, 1]$ and does not take place otherwise. This is the main difference between primary branches and secondary branches described here.

In order to continuate a secondary branch given by asymptotics (59) we again apply approximate method of Section 3.2. Taking into account that solutions $w(x)$ corresponding to g_k with $k \geq 1$ are even and $2\pi/k$-periodic, we choose $\psi = \cos(kx)$ and solve Galerkin's system (47) in a Banach subspace $X \subset C_{\rm per}([-\pi, \pi]; \mathbb{C})$ with orthogonal basis

$$1 \quad \text{and} \quad \cos(mkx), \quad m = 2, 3, \ldots.$$

Particular examples considered below reveal that each secondary branch is born in the ball Σ_0, see definition (39), then extends to the ball's boundary where it undergoes bending bifurcation and gives rise to a curve of coherence-incoherence patterns with equidistant coherent regions, e.g. $|w(x)| \geq 1$, in the incoherent background, e.g. $|w(x)| < 1$.

We want to emphasize that our analysis of secondary branches is far from being complete. For example, we did not consider k-twisted solutions described by formula (48) with $k \neq 0$. Some secondary (or even higher order) bifurcation points may also occur along numerically continuated curves of coherence-incoherence patterns, see for example recent work [30]. We plan to address these questions in our future studies.

3.6 Example: Piecewise-constant coupling

Let us consider a particular example of NEVP (28) with piecewise-constant coupling function (5). This function can be written in the form of complex Fourier series (29) with coefficients

$$g_0 = \frac{1}{2\pi} \quad \text{and} \quad g_k = g_{-k} = \frac{\sin(\pi k r)}{2\pi^2 k r}, \quad k = 1, 2, \dots .$$

First we fix coupling radius to be $r = 0.6$ and apply analytical results and numerical algorithms of Sections 3.2–3.5 to obtain a part of the NEVP's solution set that corresponds to leading Fourier coefficients g_0, g_1, g_2 and g_3. The result is shown in Fig. 5. For each solution $(\mu, w) \in$

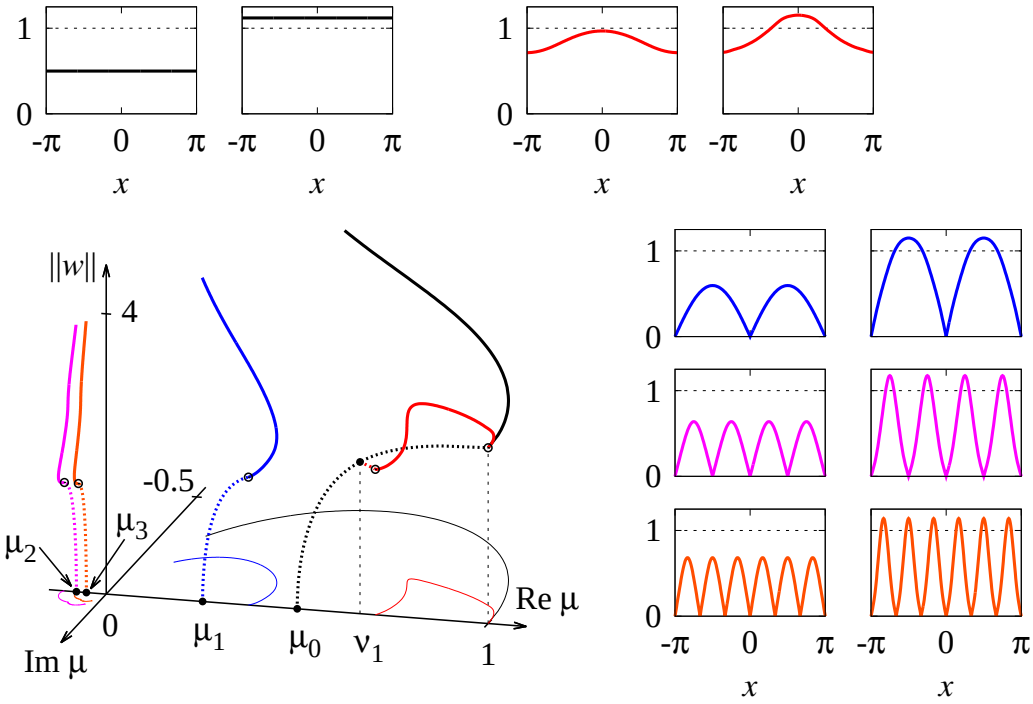

Figure 5: Solution of NEVP (28) for piecewise-constant coupling function (5) with coupling radius $r = 0.6$. Primary branches (black,blue,purple and orange thick lines) bifurcate from the trivial solution $w = 0$ at $\mu = \mu_k := \pi g_k$ where g_k are Fourier coefficients of coupling function G. The only secondary branch (red thick line) bifurcates from the primary branch of spatially uniform solutions (black thick line) at $\mu = \nu_1$, see (58). Each branch first lies in the plane $\mathrm{Im}\ \mu = 0$ (dashed lines), but after approaching a bending bifurcation point (empty circle) it turns and proceeds with complex values μ (solid lines). Thin lines show projections on the bottom plane $\|w\| = 0$ of the corresponding thick solid lines with the same color. Additional panels, using color-code of the main plot, demonstrate $|w(x)|$-profiles typical for each solution branch before (left panel) and after (right panel) the bending bifurcation point. Inequalities $|w(x)| \geq 1$ and $|w(x)| < 1$ correspond to coherent and incoherent regions, respectively. Thus all thick solid lines in the main plot (except black one) denote coherence-incoherence patterns.

$\mathbb{C} \times C_{\mathrm{per}}([-\pi, \pi]; \mathbb{C})$ we show its $3D$-projection where function w is replaced by its L^2-norm.

Thick black line (dashed and solid) displays primary branch of spatially uniform solutions (49) which bifurcates at $\mu = \mu_0$, see (53), and is described by Eqs. (50)–(51) with $k = 0$. Dashed part of the line lies within the plane $\mathrm{Im}\ \mu = 0$. When the line approaches bending bifurcation point (empty circle), it abruptly turns and leaves the plane $\mathrm{Im}\ \mu = 0$ becoming a solid line of the same color. For the convenience of $3D$-perception, we plot the projection of solid black line on the plane $\|w\| = 0$ as a thin black line. Other k-twisted solutions defined by Eqs. (50)–(51) are not shown.

In a similar way, we represent other primary (blue, purple and orange curves) and secondary (red curve) solution branches discussed in Sections 3.4 and 3.5, respectively. The primary branches bifurcate at values $\mu = \mu_k$, see (53), and the secondary branches bifurcate at values $\mu = \nu_k$, see (58). Remark an important role of the Fourier coefficients' signs. Branches appearing at $\mu_2, \mu_3 < 0$ have different location compared to those appearing at $\mu_0, \mu_1 > 0$. This means that they are observed for different values of phase lag parameter α, see formula (23). Moreover, only positive Fourier coefficient g_1 gives rise to a secondary solution branch bifurcating from the branch of spatially uniform solutions. Negative coefficients g_2, g_3 do not satisfy condition $g_k \in (0, g_0)$, therefore due to Lemma 5 they do not define bifurcation points ν_k. Taking into account that Fourier coefficients of piecewise-constant coupling function (5) change their signs for varying coupling radius r, we conclude that each secondary branch can be found for particular interval (or intervals) of r only, whereas primary branches exist for all values of coupling radius r.

Insert panels around the main plot are arranged in pairs. Using the same color-code they display typical $|w(x)|$-profiles observed along each solution branch before (left panel) and after (right panel) the corresponding bending bifurcation point marked as empty circle in the main plot. Along dashed lines (which lie in the plane $\mathrm{Im}\ \mu = 0$) we obtain $|w(x)|$-profiles with $|w(x)| < 1$, hence incoherent states. In contrary, every thick solid line of the main plot (except black one!) denotes coherence-incoherence patterns since corresponding $|w(x)|$-profiles comprise both patches of coherence $|w(x)| \geq 1$ and incoherence $|w(x)| < 1$.

3.7 Example: Cosine coupling

Let us consider another example of NEVP (28) with cosine coupling function (4). A particular feature of this function is its complex Fourier series (29) which has only three nonvanishing coefficients

$$g_0 = \frac{1}{2\pi} \quad \text{and} \quad g_1 = g_{-1} = \frac{A}{4\pi}.$$

This means that applying results of Sections 3.4 and 3.5 we obtain only two primary solution branches bifurcating at $\mu = \mu_0$ and $\mu = \mu_1$, and at most one secondary solution branch bifurcating at $\mu = \nu_1$, see formulas (53) and (58), respectively. We recall that due to Lemma 5 secondary branch exists for $g_1 \in (0, g_0)$ only, that is equivalent to condition $A \in (0, 2)$.

Remarkably, simple form of cosine coupling (4) allows us to write more explicitly primary branch bifurcating at $\mu = \mu_1$. Indeed, simple check demonstrates that function

$$w(x) = p \sin x \quad \text{where} \quad p \in (0, \infty)$$

satisfies NEVP (28), provided

$$\mu = \frac{A}{2\pi}\int_{-\pi}^{\pi} h\left(p^2\sin^2 y\right)\sin^2 y\, dy.$$

Hence this branch is completely known without any numerical continuation.

The solution set of NEVP (28) for cosine coupling function with $A = 0.9$ is shown in Fig. 6. Here we used the same color-code representation as in Fig. 5. Again thick black line denotes a

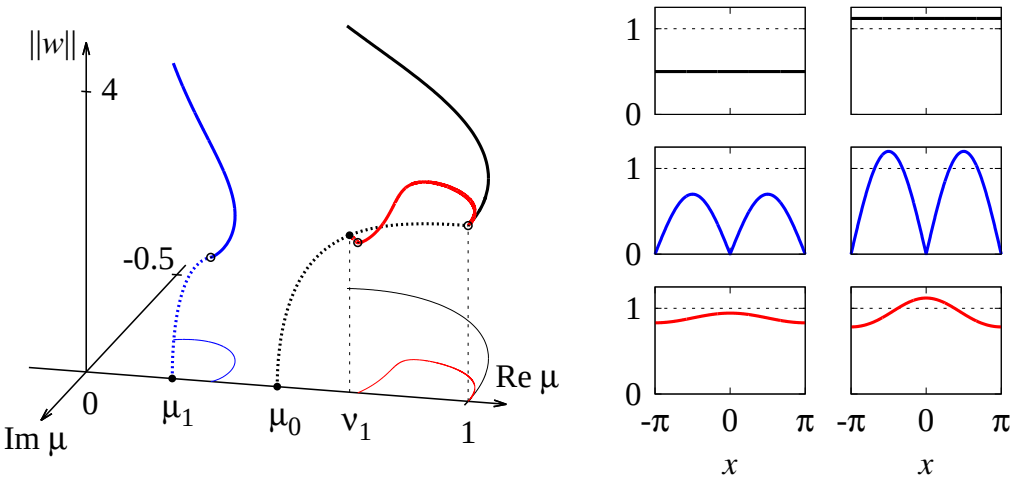

Figure 6: Solution of NEVP (28) for cosine coupling function (5) with parameter $A = 0.9$. Notations and color-code are the same as in Fig. 5.

branch of spatially uniform solutions, whereas thick blue and red lines are another primary and secondary branches, respectively. Solid parts of the curves represent dynamical regimes from Fig. 3 in accordance with the color-code of their snapshots. Thus solid blue and red lines denote two different types of coherence-incoherence patterns. Remark the anti-phase alternation between phases of neighbouring coherent regions in the coherence-incoherence pattern corresponding to primary branch, see panel with $\arg a(x)$ in Fig. 3(a). This feature is not observed in the secondary coherence-incoherence pattern, see Fig. 3(b), and apparently can be used to distinguish primary and secondary patterns in numerical simulations of system (2)–(3).

4 Stability analysis

Suppose that $z(x,t) = a(x)e^{i\Omega t}$ is one of the standing waves corresponding to a solution (μ, w) of NEVP (28), see Proposition 1. Below we consider stability properties of this standing wave within the Ott-Antonsen manifold. To this end, we use an ansatz

$$z(x,t) = (a(x) + v(x,t))e^{i\Omega t}$$

with a small perturbation v. Substituting this into Eq. (12) and linearizing the result with respect to v, we obtain

$$\frac{dv}{dt} = \eta(x)v - \frac{i}{2}e^{i\beta}\left(\mathcal{G}v + \left(e^{-i\beta}a(x)\right)^2\mathcal{G}\overline{v}\right) \tag{63}$$

where

$$\eta(x) = i\left(\omega - \Omega - e^{-i\beta}a(x)\mathcal{G}\overline{a}\right). \tag{64}$$

Applying formulas (17), (19) and (20), we rewrite coefficient η as follows

$$\eta(x) = \begin{cases} i(\omega-\Omega)\sqrt{1-|w(x)|^2} & \text{for} \quad |w(x)|<1, \\ \pm(\omega-\Omega)\sqrt{|w(x)|^2-1} & \text{for} \quad |w(x)|\geq 1, \end{cases} \tag{65}$$

where in the second line we use sign '$+$' or '$-$' depending on the choice $a(x) = a_+(x)$ or $a(x) = a_-(x)$ in the coherent region. Eq. (12) contains complex conjugated terms therefore one has to consider it not as a single complex equation, but as a short form of system of two real equations. Respectively, we have to rewrite complex Eq. (63) as a system for a two component vector-function

$$\mathbf{v}(t) = \begin{pmatrix} \mathrm{Re}\ v(x,t) \\ \mathrm{Im}\ v(x,t) \end{pmatrix} \in C_{\mathrm{per}}([-\pi,\pi];\mathbb{R}^2).$$

Then equivalent form of Eq. (63) reads

$$\frac{d\mathbf{v}}{dt} = \mathcal{L}\mathbf{v} \quad \text{where} \quad \mathcal{L} := \mathcal{M} + \mathcal{K}, \tag{66}$$

and $\mathcal{M} \ : \ C_{\mathrm{per}}([-\pi,\pi];\mathbb{R}^2) \to C_{\mathrm{per}}([-\pi,\pi];\mathbb{R}^2)$ is a multiplication operator

$$(\mathcal{M}\mathbf{v})(x) := \mathbf{M}(x)\mathbf{v} \quad \text{with} \quad \mathbf{M}(x) := \begin{pmatrix} \mathrm{Re}\ \eta(x) & -\mathrm{Im}\ \eta(x) \\ \mathrm{Im}\ \eta(x) & \mathrm{Re}\ \eta(x) \end{pmatrix}, \tag{67}$$

whereas $\mathcal{K} \ : \ C_{\mathrm{per}}([-\pi,\pi];\mathbb{R}^2) \to C_{\mathrm{per}}([-\pi,\pi];\mathbb{R}^2)$ is an integral operator

$$(\mathcal{K}\mathbf{v})(x) := \int_{-\pi}^{\pi} \mathbf{K}(x,y)\mathbf{v}(y)dy$$

with a matrix kernel given by

$$\mathbf{K}(x,y) = \frac{1}{2}\mathbf{Q}\mathbf{P}(x)G(x-y) \tag{68}$$

where for the sake of shortage we used notations

$$\mathbf{P}(x) = \begin{pmatrix} \mathrm{Re}\left(1+\left(e^{-i\beta}a(x)\right)^2\right) & -\mathrm{Im}\left(1-\left(e^{-i\beta}a(x)\right)^2\right) \\ \mathrm{Im}\left(1+\left(e^{-i\beta}a(x)\right)^2\right) & \mathrm{Re}\left(1-\left(e^{-i\beta}a(x)\right)^2\right) \end{pmatrix} \tag{69}$$

and

$$\mathbf{Q} = \begin{pmatrix} \sin\beta & \cos\beta \\ -\cos\beta & \sin\beta \end{pmatrix}.$$

Linear operator $\mathcal{L}$ is time-independent, hence based on the location of its spectrum $\sigma(\mathcal{L})$ we can make a conclusion about the stability of corresponding standing wave $a(x)e^{i\Omega t}$. It is easy to

see that for piecewise-smooth coupling function G and continuous wave amplitude a both operators $\mathcal{M}$ and $\mathcal{K}$ are bounded linear operators in $C_{\rm per}([-\pi,\pi];\mathbb{R}^2)$. Moreover, definition (68) implies that integral operator $\mathcal{K}$ is compact in $C_{\rm per}([-\pi,\pi];\mathbb{R}^2)$. Following general spectral theory of linear operators in Banach space [47], we distinguish two parts in the spectrum $\sigma(\mathcal{L})$. The *point spectrum* $\sigma_{\rm pt}(\mathcal{L}) \subset \sigma(\mathcal{L})$ consists of all complex numbers λ such that $\lambda\mathcal{I} - \mathcal{L}$ is a Fredholm operator of index zero. In other words, each $\lambda \in \sigma_{\rm pt}(\mathcal{L})$ is an isolated eigenvalue of finite multiplicity. The complement of discrete spectrum we call *essential spectrum* and denote it as $\sigma_{\rm ess}(\mathcal{L})$.

For multiplication operator $\mathcal{M}$, it is known [48] that it has only essential spectrum consisting of all $\lambda \in \mathbb{C}$ such that

$$\det \begin{pmatrix} \lambda - \mathrm{Re}\ \eta(x) & \mathrm{Im}\ \eta(x) \\ -\mathrm{Im}\ \eta(x) & \lambda - \mathrm{Re}\ \eta(x) \end{pmatrix} = 0 \quad \text{for some} \quad x \in [-\pi,\pi], \tag{70}$$

therefore

$$\sigma(\mathcal{M}) = \sigma_{\rm ess}(\mathcal{M}) = \Big\{ \eta(x) \ : \ -\pi \le x \le \pi \Big\} \cup \{c.c.\}\,, \tag{71}$$

where $\{c.c.\}$ denotes the complex conjugate of the previous set. Essential spectrum is invariant under compact perturbations [49], hence $\sigma_{\rm ess}(\mathcal{L}) = \sigma_{\rm ess}(\mathcal{M})$. The remaining point spectrum $\sigma_{\rm pt}(\mathcal{L})$ has no simple representation but can be calculated numerically as we explain below. Anyhow for bounded compact operator $\mathcal{K}$ it is always known [48] that

$$\sigma_{\rm pt}(\mathcal{L}) \subset \Big\{ \lambda \in \mathbb{C} \ : \ \mathrm{dist}(\lambda, \sigma_{\rm ess}(\mathcal{M})) \le \|\mathcal{K}\| \Big\}\,. \tag{72}$$

For every coherence-incoherence pattern found as a solution of NEVP (28), formula (65) gives either real or pure imaginary values of $\eta(x)$. Hence according to formula (71) such coherence-incoherence pattern has a T-shaped essential spectrum $\sigma_{\rm ess}(\mathcal{L})$ with a symmetric interval of neutral eigenvalues corresponding to incoherent region. Another interval corresponds to coherent region and consists solely of real eigenvalues, which all lie either in the left or in the right complex half-plane, see Fig. 7(a) and (b). On the other hand, sign of $\mathrm{Re}\ \eta(x)$ is determined by the choice of $a = a_+$ or $a = a_-$ in coherent region. Therefore we easily verify that only two of four standing waves given by Proposition 1 have stable essential spectrum.

Proposition 2 *Suppose that (μ, w) is a solution of NEVP (28) which has coherent $|w(x)| \ge 1$ as well as incoherent $|w(x)| < 1$ regions. Then standing waves (15) given by*

$$\Omega = \omega - |\mu|, \quad a(x) = h\left(|w(x)|^2\right) w(x) \quad \textit{with} \quad \beta = -\arg\mu$$

and

$$\Omega = \omega + |\mu|, \quad a(x) = \overline{h}\left(|w(x)|^2\right) \overline{w}(x) \quad \textit{with} \quad \beta = \pi + \arg\mu$$

have stable essential spectrum, whereas the other two standing waves mentioned in Proposition 1 are always unstable (at least because of the location of their essential spectrum).

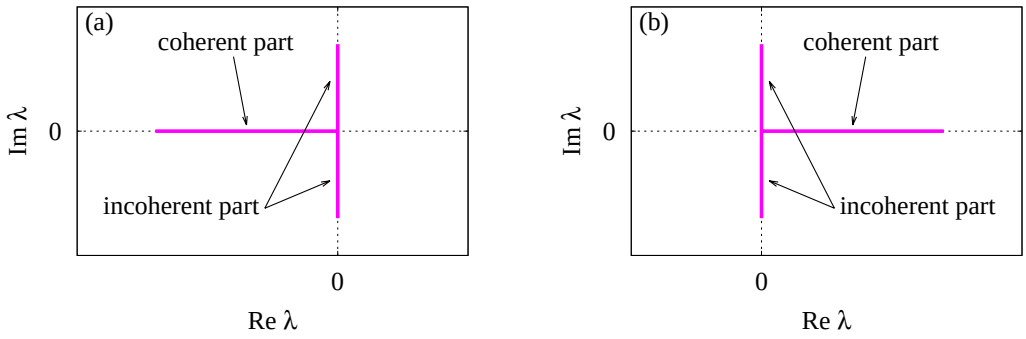

Figure 7: Two forms of essential spectrum calculated by formulas (65) and (71) for a coherence-incoherence pattern. The interval along real axis and the other one along imaginary axis are due to coherent $|w(x)| \geq 1$ and incoherent $|w(x)| < 1$ parts, respectively. The real part of the spectrum is stable (a) or unstable (b) depending on the choice of sign '$-$' or '$+$' in the second line of Eq. (65).

Remark 3 *Most of classical bifurcations can be inferred from the spectrum of corresponding linearized operator. For example, Hopf bifurcation occurs when a pair of complex-conjugate eigenvalues crosses the imaginary axis. Similar criterion exists for Turing bifurcation when one looks for an intersection between the imaginary axis and continuous spectrum. In this context, formulas (65) and (71) clarify spectral behaviour typical for the bending bifurcation defined at the end of Section 3.2. At this bifurcation point a new coherent region, e.g.* $|w(x)| \geq 1$*, appears in the incoherent surrounding, e.g.* $|w(x)| < 1$*. Respectively, due to Eq. (65) essential spectrum* $\sigma_{\rm ess}(\mathcal{L})$ *gets a new portion of stable/unstable spectrum protruding at the zero from its neutral part.*

Stability analysis of standing wave (15) also relies on the analysis of corresponding point spectrum $\sigma_{\rm pt}(\mathcal{L})$. The latter consists of all $\lambda \in \mathbb{C}$ such that equation

$$(\lambda \mathcal{I} - \mathcal{M} - \mathcal{K})\,\mathbf{v} = 0 \tag{73}$$

has a non-trivial solution $\mathbf{v} \in C_{\rm per}([-\pi, \pi]; \mathbb{R}^2)$. Note for $\lambda \notin \sigma_{\rm ess}(\mathcal{L})$, spectral equation (73) can be rewritten in a more convenient form

$$\mathbf{v} = (\lambda \mathbf{I} - \mathbf{M}(x))^{-1} (\mathcal{K}\mathbf{v})(x) \tag{74}$$

where $\mathbf{I}$ is the two-dimensional identity matrix and $\mathbf{M}$ is given by (67). In order to solve Eq. (74) we apply the following approximate scheme. Taking into account operator convergence (32) we replace compact operator $\mathcal{K}$ with its finite-rank approximation of the form

$$\begin{aligned} (\mathcal{K}\mathbf{v})(x) &\approx \int_{-\pi}^{\pi} \frac{1}{2} \mathbf{Q}\mathbf{P}(x) G_K(x-y) \mathbf{v}(y) dy \\ &= \frac{1}{2} \mathbf{Q}\mathbf{P}(x) \sum_{k=-K}^{K} g_k e^{ikx} \langle e^{ikx}, \mathbf{v} \rangle \end{aligned} \tag{75}$$

where G_K is given by a truncated Fourier sum (31) with sufficiently large K, and for every $\mathbf{v} = (v_1, v_2)^T$ we use a notation

$$\langle e^{ikx}, \mathbf{v}\rangle = \begin{pmatrix} \langle e^{ikx}, v_1\rangle \\ \langle e^{ikx}, v_2\rangle \end{pmatrix}.$$

Then substituting (75) into Eq. (74) and calculating $2K+1$ non-vanishing Fourier projections we obtain a system

$$\langle e^{ijx}, \mathbf{v}\rangle = \sum_{k=-K}^{K} \mathbf{B}_{jk}(\lambda)\langle e^{ikx}, \mathbf{v}\rangle, \quad j = -K, \ldots, K, \tag{76}$$

where

$$\mathbf{B}_{jk}(\lambda) := \frac{1}{2} g_k \left\langle e^{ijx}, e^{ikx}(\lambda \mathbf{I} - \mathbf{M}(x))^{-1}\mathbf{Q}\mathbf{P}(x)\right\rangle.$$

Obviously, Eqs. (76) have a nontrivial solution $\langle e^{ikx}, \mathbf{v}\rangle$, $k = -K, \ldots, K$, if and only if λ satisfies a characteristic equation

$$\chi(\lambda) := \det\left(\mathbf{I} - \mathbf{B}(\lambda)\right) = 0 \tag{77}$$

with a $(4K+2)$-dimensional square matrix given by

$$\mathbf{B}(\lambda) := \begin{pmatrix} \mathbf{B}_{(-K)(-K)}(\lambda) & \mathbf{B}_{(-K)(-K+1)}(\lambda) & \ldots & \mathbf{B}_{(-K)K}(\lambda) \\ \mathbf{B}_{(-K+1)(-K)}(\lambda) & \mathbf{B}_{(-K+1)(-K+1)}(\lambda) & \ldots & \mathbf{B}_{(-K+1)K}(\lambda) \\ \vdots & \vdots & \ddots & \vdots \\ \mathbf{B}_{K(-K)}(\lambda) & \mathbf{B}_{K(-K+1)}(\lambda) & \ldots & \mathbf{B}_{KK}(\lambda) \end{pmatrix}.$$

It is easy to see that each matrix $\mathbf{B}_{jk}(\lambda)$ is an analytic function of λ in $\mathbb{C}\backslash\sigma_{\rm ess}(\mathcal{L})$. Hence the same is true for function $\chi(\lambda)$ from Eq. (77). Thus taking into account spectral radius estimate (72) and the fact that the zeros of an analytic function are always isolated, we may expect to find at most a finite number of solutions to Eq. (77). These solutions determine only approximate point spectrum. However, operator convergence (32) insures that using in (75) functions G_K with larger K we obtain increasingly better approximations of $\sigma_{\rm pt}(\mathcal{L})$.

4.1 Example: Cosine coupling

Let us consider two coherence-incoherence patterns, see Fig. 6, which were obtained as primary and secondary solution branches of NEVP (28) with cosine coupling function (4). Then applying Proposition 2 for each (μ, w) we construct standing waves (15) corresponding to these patterns. Such waves have stable essential spectrum, Fig. 7(a), but may have stable or unstable point spectrum. Note that Fourier series of cosine coupling function contains only three nonvanishing harmonics therefore in order to calculate the point spectrum we don't need to approximate G. Indeed already for $K = 1$ characteristic equation (77) is exact. Solving this equation numerically we found only a finite number of eigenvalues in point spectrum. Based on

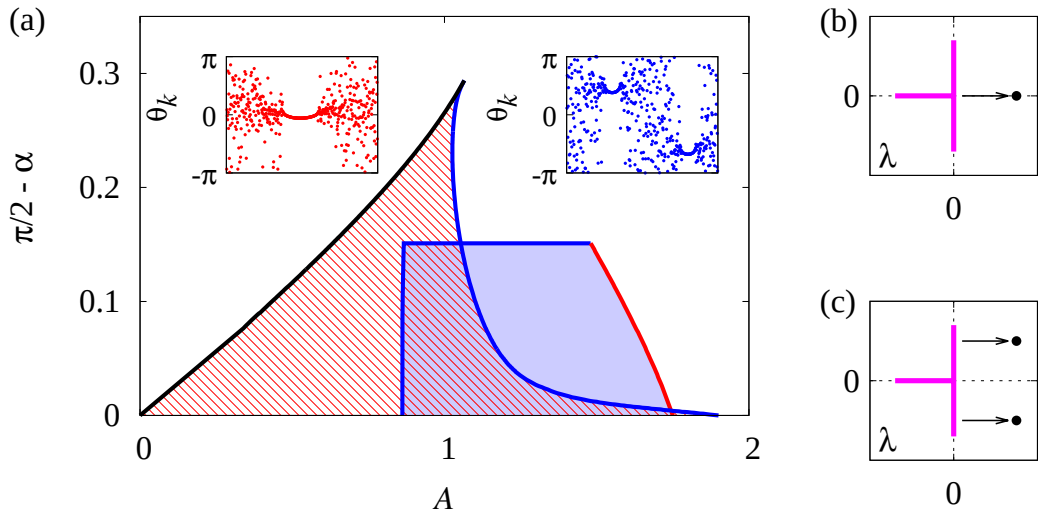

Figure 8: Bifurcation diagram (a) for two coherence-incoherence patterns corresponding to primary (inset panel with blue dots) and secondary (inset panel with red dots) solution branches of NEVP (28) with cosine coupling function (4), see Fig. 6. The former solution is stable in blue region, and the latter is stable in hatched region. Black line denotes fold bifurcation. Red and blue stability boundaries correspond to the cases when a single real (b) or a pair of complex conjugate (c) eigenvalues appear from essential spectrum (T-shaped purple line).

their analysis we found stability regions of primary (blue) and secondary (hatched) coherence-incoherence patterns. As expected (recall Fig. 3(a) and (b)) there is a considerable overlap of the regions indicating parameter values where multistability is favoured. The boundaries of stability regions are of two qualitatively different types. Red line corresponds to the case of single real eigenvalue appearing from essential spectrum, whereas blue lines denote Hopf-like boundaries where a pair of complex conjugate eigenvalues bifurcates from essential spectrum.

5 Discussion

In present work we formulated a general approach for bifurcation analysis of coherence-incoherence patterns observed in system (2)–(3). We rely on the assumption that in the large N limit such patterns are described by standing wave solutions of Eq. (12). The assertion is based on the continuum limit representation and the Ott-Antonsen invariant manifold reduction available in the case of sinusoidally coupled phase oscillators. Importantly, each standing wave solution of Eq. (12) has clear interpretation in terms of local order parameter which demarcates coherent and incoherent regions of corresponding pattern.

Our approach includes two main steps. First, given a coupling function G we solve NEVP (28), which plays the role of self-consistency equation for spatial amplitude of unknown standing wave and its collective frequency. Second, applying Proposition 2 we transform every solution of NEVP (28) into two standing waves and perform their stability analysis with respect to Eq. (12). The waves are always neutrally stable due to the location of their essential spectrum, but may

be stable or not with respect to the location of their point spectrum. Both spectral components are determined by time-independent operator $\mathcal{L}$ appearing in the right-hand side of linearized Eq. (66). More precisely, essential spectrum of $\mathcal{L}$ is known explicitly, whereas point spectrum of $\mathcal{L}$ can be calculated using approximate algorithm of Section 4.

Already in the first step we obtain a plethora of useful information about standing wave solutions of Eq. (12) from the Fourier series of coupling function G. In particular, we showed that every non-zero Fourier coefficient g_k, $k \geq 1$, is responsible for appearance of two qualitatively different primary branches in the solution set of NEVP (28). The first branch describes so-called k-twisted solutions of original system (2)–(3), while the second branch includes standing waves corresponding to $(2\pi/k)$-periodic coherence-incoherence patterns. Note that moving along the latter branch we find coherence-incoherence patterns only beyond a particular point which we refer to as bending bifurcation point. Another interesting fact is, that sign of g_k indicates whether corresponding coherence-incoherence pattern exists for $\alpha \in (-\pi/2, \pi/2)$, if $g_k > 0$, or for $\alpha \in (\pi/2, 3\pi/2)$, if $g_k < 0$. However, the pattern's stability is still determined by point spectrum of corresponding linearized operator $\mathcal{L}$.

The primary branch corresponding to the leading Fourier coefficient $g_0 \neq 0$ describes spatially uniform solutions of Eq. (12). Its larger part represents the completely coherent state of original system (2)–(3). If for some g_k, $k \geq 1$, we get $g_k/g_0 \in (0, 1]$, then along this primary branch there exists a bifurcation point giving rise to a secondary branch in the solution set of NEVP (28). Moving along the secondary branch beyond its bending bifurcation point we obtain another $(2\pi/k)$-periodic coherence-incoherence pattern. Particular examples considered above illustrate a series of qualitative differences between primary and secondary coherence-incoherence patterns. The solution curve of NEVP (28) corresponding to secondary patterns looks as a half-loop starting and ending at the primary branch of spatially uniform solutions, therefore one usually finds on it a fold bifurcation point, see red lines in Figs. 5 and 6. In contrast, the solution curve of NEVP (28) corresponding to primary patterns simply extends to infinity, see all lines except red in Figs. 5 and 6. Another difference refers to the fact that $|w(x)|$-profile of primary pattern approaches zero for some $x \in [-\pi, \pi]$, see insert panels in Figs. 5 and 6. As a result, neighbouring coherent regions turn out to be in anti-phase, see panel with $\arg a(x)$ in Fig. 3(a).

It is a surprising fact that almost all previous studies related to the topic reported only on the secondary coherence-incoherence pattern corresponding to the first Fourier coefficient g_1, see for example [12, 14, 15, 19, 20]. The primary pattern corresponding to g_1 was found much later in [28]. Therefore we conjecture that most of the patterns described above still wait for their observation. A good illustration for them could be coherence-incoherence patterns found numerically by Y. Maistrenko [50] in system (2)–(3) with piecewise-constant coupling function (5) and $\alpha \approx \pi$ (so-called repulsive coupling case). However their classification goes beyond the scope of this paper.

For effective numerical search of new coherence-incoherence patterns one also has to know their stability boundaries, e.g. the second step of our bifurcation analysis scheme. In this paper we calculated such boundaries in the simplest case of cosine coupling only, see Fig. 8. Even this particular result turns out to be instructive, since we encounter two new types of stability boundaries, see Fig. 8(b) and (c), which to the best of our knowledge were not reported before.

This and other facts clearly demonstrate how far is our knowledge of coherence-incoherence patterns from being complete. In this context, we believe that our work helps to understand better this complex phenomenon and shows promising directions for future research.

Acknowledgments

I would like to thank M. Wolfrum, A. Pikovsky and Y. Maistrenko for many helpful discussions.

References

[1] W. Singer. Synchronization of cortical activity and its putative role in information processing and learning. *Ann. Rev. Physiol.*, 55:349–374, 1993.

[2] C. M. Gray. Synchronous oscillations in neuronal systems: mechanisms and functions. *J. Comput. Neurosci.*, 1:11–38, 1994.

[3] S. Farmer. Neural rhythms in Parkinson's disease. *Brain*, 125:1175–1176, 2002.

[4] A. F. Taylor, M. R. Tinsley, F. Wang, Z. Huang, and K. Showalter. Dynamical quorum sensing and synchronization in large populations of chemical oscillators. *Science*, 323:614–617, 2009.

[5] A. F. Taylor, S. Nkomo, and K. Showalter. Chimera and phase-cluster states in populations of coupled chemical oscillators. *Nature Physics*, 8:662–665, 2012.

[6] K. Wiesenfeld and J. W. Swift. Averaged equations for Josephson junction series arrays. *Phys. Rev. E*, 51:1020–1025, 1995.

[7] H. Haus. Modelocking of lasers. *IEEE J. Sel. Top. Quantum Electron.*, 6:1173–1185, 2000.

[8] A. Pikovsky, M. Rosenblum, and J. Kurths. *Synchronization, a universal concept in nonlinear sciences*. Cambridge University Press, Cambridge, 2001.

[9] Y. Kuramoto. *Chemical Oscillations, Waves, and Turbulence*. Springer, Berlin Heidelberg New York, 1984.

[10] F. C. Hoppensteadt and E. M. Izhikevich. *Weakly Connected Neural Networks*. Springer, Berlin Heidelberg New York, 1997.

[11] H. Sakaguchi and Y. Kuramoto. A soluble active rotater model showing phase transitions via mutual entertainment. *Prog. Theor. Phys.*, 76:576, 1986.

[12] Y. Kuramoto and D. Battogtokh. Coexistence of coherence and incoherence in nonlocally coupled phase oscillators. *Nonlinear Phenom. Complex Syst.*, 5:380–385, 2002.

[13] S. I. Shima and Y. Kuramoto. Rotating spiral waves with phase-randomized core in nonlocally coupled oscillators. *Phys. Rev. E*, 69:036213, 2004.

[14] D. M. Abrams and S. H. Strogatz. Chimera states for coupled oscillators. *Phys. Rev. Lett.*, 93:174102, 2004.

[15] D. M. Abrams and S. H. Strogatz. Chimera states in a ring of nonlocally coupled oscillators. *Int. J. Bif. and Chaos*, 16:21–37, 2006.

[16] H. Sakaguchi. Instability of synchronized motion in nonlocally coupled neural oscillators. *Phys. Rev. E*, 73:031907, 2006.

[17] G. C. Sethia, A. Sen, and F. M. Atay. Clustered chimera states in delay-coupled oscillator systems. *Phys. Rev. Lett.*, 100:144102, 2008.

[18] O. E. Omel'chenko, Y. L. Maistrenko, and P. A. Tass. Chimera states: the natural link between coherence and incoherence. *Phys. Rev. Lett.*, 100:044105, 2008.

[19] C. R. Laing. Chimera states in heterogeneous networks. *Chaos*, 19:013113, 2009.

[20] C. R. Laing. The dynamics of chimera states in heterogeneous Kuramoto networks. *Physica D*, 238:1569–1588, 2009.

[21] E. A. Martens, C. R. Laing, and S. H. Strogatz. Solvable model of spiral wave chimeras. *Phys. Rev. Lett.*, 104:044101, 2010.

[22] G. Bordyugov, A. Pikovsky, and M. Rosenblum. Self-emerging and turbulent chimeras in oscillator chains. *Phys. Rev. E*, 82:035205, 2010.

[23] O. E. Omel'chenko, M. Wolfrum, and Y. L. Maistrenko. Chimera states as chaotic spatiotemporal patterns. *Phys. Rev. E*, 81:065201, 2010.

[24] O. E. Omel'chenko, Y. L. Maistrenko, and P. A. Tass. Chimera states induced by spatially modulated delayed feedback. *Phys. Rev. E*, 82:066201, 2010.

[25] M. Wolfrum and O. E. Omel'chenko. Chimera states are chaotic transients. *Phys. Rev. E*, 84:015201, 2011.

[26] M. Wolfrum, O. E. Omel'chenko, S. Yanchuk, and Y. L. Maistrenko. Spectral properties of chimera states. *Chaos*, 21:013112, 2011.

[27] C. R. Laing. Fronts and bumps in spatially extended Kuramoto networks. *Physica D*, 240:1960–1971, 2011.

[28] Y. Zhu, Y. Li, M. Zhang, and J. Yang. The oscillating two-cluster chimera state in non-locally coupled phase oscillators. *EPL*, 97:10009, 2012.

[29] O. E. Omel'chenko, M. Wolfrum, S. Yanchuk, Y. Maistrenko, and O. Sudakov. Stationary patterns of coherence and incoherence in two-dimensional arrays of non-locally-coupled phase oscillators. *Phys. Rev. E*, 85:036210, 2012.

[30] M. J. Panaggio and D. M. Abrams. Chimera states on a flat torus. *Phys. Rev. Lett.*, 110:094102, 2013.

[31] D. M. Abrams, R. Mirollo, S. H. Strogatz, and D. A. Wiley. Solvable model for chimera states of coupled oscillators. *Phys. Rev. Lett.*, 101:084103, 2008.

[32] E. A. Martens. Bistable chimera attractors on a triangular network of oscillator populations. *Phys. Rev. E*, 82:016216, 2010.

[33] I. Omelchenko, Y. Maistrenko, P. Hövel, and E. Schöll. Loss of coherence in dynamical networks: Spatial chaos and chimera states. *Phys. Rev. Lett.*, 106:234102, 2011.

[34] A. M. Hagerstrom, T. E. Murphy, R. Roy, P. Hövel, I. Omelchenko, and E. Schöll. Experimental observation of chimeras in coupled-map lattices. *Nature Physics*, 8:658–661, 2012.

[35] D. A. Wiley, S. H. Strogatz, and M. Girvan. The size of the sync basin. *Chaos*, 16:015103, 2006.

[36] T. Girnyk, M. Hasler, and Y. Maistrenko. Multistability of twisted states in non-locally coupled Kuramoto-type models. *Chaos*, 22:013114, 2012.

[37] E. Luçon and W. Stannat. Mean field limit for disordered diffusions with singular interactions. *arXiv:1301.6521*, 2013.

[38] J. D. Crawford and K. T. R. Davies. Synchronization of globally coupled phase oscillators: singularities and scaling for general couplings. *Physica D*, 125:1–46, 1999.

[39] R. Mirollo and S. H. Strogatz. The spectrum of the partially locked state for the Kuramoto model. *J. Nonlinear Sci.*, 17:309–347, 2007.

[40] E. Ott and T. M. Antonsen. Low dimensional behavior of large systems of globally coupled oscillators. *Chaos*, 18:037113, 2008.

[41] E. Ott and T. M. Antonsen. Long time evolution of phase oscillator systems. *Chaos*, 19:023117, 2009.

[42] S. Watanabe and S. H. Strogatz. Constants of motion for superconducting Josephson arrays. *Physica D*, 74:197–253, 1994.

[43] A. Pikovsky and M. Rosenblum. Partially integrable dynamics of hierarchical populations of coupled oscillators. *Phys. Rev. Lett.*, 101:264103, 2008.

[44] S. H. Strogatz. From Kuramoto to Crawford: exploring the onset of synchronization in populations of coupled oscillators. *Physica D*, 143:1–20, 2000.

[45] M. A. Krasnoselski. *Topological Methods in the Theory of Nonlinear Integral Equations*. Macmillan, New Jork, 1965.

[46] P. H. Rabinowitz. Some global results for nonlinear eigenvalue problems. *J. Functional Analysis*, 7:487–513, 1971.

[47] D. E. Edmunds and W. Evans. *Spectral theory and differential operators*. Oxford University Press, Oxford, 1987.

[48] E. A. Biberdorf and M. Vath. On the spectrum of orthomorphisms and Barbashin operators. *Journal for Analysis and its Applications*, 18:859–873, 1999.

[49] T. Kato. *Perturbation theory for linear operators*. Springer, Berlin Heidelberg New York, 1966.

[50] Y. Maistrenko. Chimera states for repulsively coupled phase oscillators. In B. Mehlig, O. Ghavami, S. Östlund, and D. Hanstorp, editors, *XXXII Dynamics Days Europe: Book of Abstracts*, page 35, Gothenburg, Sweden, 2012. University of Gothenburg.